

**DESIGN AND DEVELOPMENT OF LATEX CUPS COLLECTOR ROBOT
(MECHANICAL)**

KHOR XI BO

**A project report submitted in partial fulfilment of the
requirements for the award of the degree of
Bachelor of Engineering (Honours) Industrial Engineering**

**Faculty of Engineering and Green Technology
Universiti Tunku Abdul Rahman**

May 2022

DECLARATION

I hereby declare that this project report is based on my original work except for citations and quotations which have been duly acknowledged. I also declare that it has not been previously and concurrently submitted for any other degree or award at UTAR or other institutions.

Signature :

Handwritten signature of Khor Xi Bo in black ink, featuring stylized Chinese characters and the letters 'XIBO'.

Name : Khor Xi Bo

ID No. : 17AGB03672

Date : 14/4/2022

APPROVAL FOR SUBMISSION

I certify that this project report entitled “**DESIGN AND DEVELOPMENT OF LATEX CUPS COLLECTOR ROBOT (MECHANICAL)**” was prepared by **KHOR XI BO** has met the required standard for submission in partial fulfilment of the requirements for the award of Bachelor of Engineering (Honours) Industrial Engineering at Universiti Tunku Abdul Rahman.

Approved by,

Signature : 
Supervisor : Dr. Lim Chong Hooi
Date : 13/4/22

Signature : 
Co-Supervisor : Ts. Tan Yee Chyan
Date : 14/4/22

The copyright of this report belongs to the author under the terms of the copyright Act 1987 as qualified by Intellectual Property Policy of Universiti Tunku Abdul Rahman. Due acknowledgement shall always be made of the use of any material contained in, or derived from, this report.

© 2022, KHOR XI BO. All right reserved.

Specially dedicated to
my beloved parents, siblings, and friends

ACKNOWLEDGEMENTS

I would like to thank everyone who had contributed to the successful completion of this project. I would like to express my gratitude to my research supervisor, Dr. Lim Chong Hooi for his invaluable advice, guidance, and his enormous patience throughout the development of the research.

In addition, I would also like to express my gratitude to my loving parents and friends who had helped and given me encouragement.

**DESIGN AND DEVELOPMENT OF LATEX CUPS COLLECTOR ROBOT
(MECHANICAL)**

ABSTRACT

Due to the growing demand, the products coming from rubber plantations, such as gloves, tires, and mattresses, are highly sought after. However, due to several factors, world rubber production has reduced in recent years, especially in Malaysia. In this project, an automated prototype robot for collecting latex cups was built to help workers in the latex collection process. This robot is constructed on a mobile platform based on a rear-wheel drive, double wishbone suspension, and Ackermann's steering transmission, with a motor-driven Four Degree of Freedom (DoF) manipulator arm and a latex storage tank located on the platform. For the movement of the robot transmission and manipulator arm, ultrasonic sensors and a camera are employed to locate the position of rubber trees and latex cups, respectively. The Arduino Uno and the motor driver circuit are used as the controllers of this robot. The developed prototype robot has undergone prototype test runs to verify the control system, as well as the robot's mobility test, static test, and balance test, and to test the stability of the robot platform. Those results showed that the prototype design is feasible and is able to perform basic tasks automatically in the unstructured terrain of the rubber plantation. In addition, this prototype can act as a basic design for future development.

TABLE OF CONTENTS

DECLARATION	ii
APPROVAL FOR SUBMISSION	iii
ACKNOWLEDGEMENTS	vi
ABSTRACT	vii
TABLE OF CONTENTS	viii
LIST OF TABLES	xi
LIST OF FIGURES	xii
LIST OF SYMBOLS / ABBREVIATIONS	xvii

CHAPTER

1	INTRODUCTION	1
	1.1 Background	1
	1.2 Problem Statements	2
	1.3 Aims and Objectives	4
	1.4 Scope of Project	5
	1.5 Outline of Report	5
2	LITERATURE REVIEW	6
	2.1 Introduction to Latex	6
	2.2 Agricultural Robot in Harvesting Process	7
	2.3 Challenges faced to Introduce Agricultural Robot	8
	2.4 Components of Agricultural Robot	9
	2.4.1 Sensing	10
	2.4.2 Planning	11
	2.4.3 Mobility	11

	2.4.4	Manipulation	11
2.5		Design concepts	12
	2.5.1	Design concepts for mobility	13
	2.5.2	Design concepts for manipulation	19
	2.5.3	Design concepts for storage tank	21
3		METHODOLOGY	22
3.1		Chosen Design	22
3.2		Prototype Design and Material Selection	23
	3.2.1	PLA Material in Solidworks Software	23
	3.2.2	Locomotion Design (Wheels)	24
	3.2.3	Transmission Design (Differential)	25
	3.2.4	Suspension Design (Double wishbone and spring)	27
	3.2.5	Steering Design (Ackermann Mechanism)	29
	3.2.6	Manipulator Design	33
	3.2.7	End effector Design (Gripper)	36
	3.2.8	Storage Tank Design	37
	3.2.9	Electric components storage board	39
	3.2.10	Base Storage Compartment	41
	3.2.11	Solidworks Assembly	41
3.3		Firmware configuration	43
	3.3.1	Parameter calculation	45
3.4		Static Analysis	51
	3.4.1	Robot Platform	51
	3.4.2	Robotic Arm	55
3.5		Centre of mass: Toppling analysis	56
	3.5.1	Centre of mass identification	56
	3.5.2	Topple Angle	58
3.6		Motion Study	59
	3.6.1	Motor Feature	60
	3.6.2	Spring Feature	61
	3.6.3	Contact Feature	62
3.7		Fabrication of Prototype and Experiment Set up	63

3.7.1	Experiment setup	64
3.8	Project Planning and Milestone	67
4	RESULTS AND DISCUSSIONS	71
4.1	Latex Cup Collector Robot prototype	71
4.2	Finite Element Analysis (Static Test)	73
4.2.1	Robot Platform	73
4.2.2	Robotic Arm	76
4.3	Centre of Mass: Toppling Analysis	78
4.3.1	Centre of mass	78
4.3.2	Topple Angle	80
4.4	Prototype test run	82
4.4.1	Functional test	82
4.4.2	Manipulator Test	85
4.5	Mobility Test	86
4.5.1	Motion Study	86
4.5.2	Mobility test run	88
4.6	Key Findings	90
5	CONCLUSION AND RECOMMENDATIONS	91
5.1	Conclusion	91
5.2	Recommendations	92
	REFERENCES	93

LIST OF TABLES

TABLE	TITLE	PAGE
3.1	Chosen means of each subfunction for the design	22
3.2	Firmware selection and its specification	44
3.3	Loads acting on the robot platform	52
3.4	Weight of each part of robotic arm	53
3.5	Four scenarios of centre of mass identification	58
4.1	Centre of mass of designed robot for 4 different scenarios	79
4.2	Calculated topple angles for four different scenarios	80
4.3	Calculated and Experimental topple angles and their % error	81
4.4	Step-by-step action and its cycle time	84

LIST OF FIGURES

FIGURE	TITLE	PAGE
1.1	Malaysia's Rubber Production and Consumption (in thousand tonnes), 2017-2021 (Source: MRC 2021 cited in IRSG, 2021)	3
2.1	The rubber tree tapping process (Source: FAO, 1977)	7
2.2	Structure of Robot System to Perform Agricultural Task (Source: Pant et al., 2019)	10
2.3	Example of leg locomotion system (Source: Oliveira et al., 2021)	13
2.4	RT Mover (source: Nakajima, 2011)	14
2.5	Transformable mobile robot with six wheels (Source: Kim, Jeon, and Yang, 2017)	14
2.6	Ackermann steering principle (Anon., n.d.)	17
2.7	Different rotation velocities of the four wheels produce the resultant turning angle for the overall robot. (Source: Wang et al., 2015)	18
2.8	Rocker-bogie suspension system (Source: Yadav, Bhardwaj and Bhardwaj, 2015)	19
3.1	Material properties of PLA plastic input in Solidworks	23
3.2	Rear wheel design in Solidworks	24
3.3	Front wheel design in Solidworks	24
3.4	Differential gear design in Solidworks	25
3.5	Rear axle with differential gear mounted with rear wheels	26

3.6	Universal joint design in Solidworks	26
3.7	Differential transmission design in Solidworks software (Side view)	26
3.8	Shock damper in (a) uncompressed and (b) compressed states.	27
3.9	Double wishbone suspension system used in the front wheel part. (a) When both sides are in the origin position; (b) When only one shock damper is compressed	28
3.10	Compression spring used in rear wheel part	28
3.11	Re-design of the spring suspension part (rear)	29
3.12	Wheel hub design in Solidworks	30
3.13	Ball joint design in Solidworks	30
3.14	Ball joint linkage rods used to connect the steering bar and wheel hubs	31
3.15	The servo motor is set to its default position (wheels are aligned straight)	31
3.16	The servo motor rotates its shaft in a clockwise direction (both wheels turn right)	32
3.17	The servo motor rotates its shaft in an anti-clockwise direction (both wheels turn left)	32
3.18	EEZYbotARM MK2 (Source: Carlo, F., 2018)	33
3.19	Manipulator base design in Solidworks	34
3.20	Horizontal arm driver lever	34
3.21	Manipulator main arm design in Solidworks	35
3.22	Horizontal arm design in Solidworks	35
3.23	Gripper support design in Solidworks	35
3.24	Gripper end-effector design	36
3.25	DC motor holder and Gripper holder designs	37
3.26	Gripper set is rotated by using the gear mechanism	37

3.27	Storage tank and its supporting parts design in Solidworks	38
3.28	Storage tank fits into the slots on the robot platform	39
3.29	Reinforcement design under the robot platform	39
3.30	(a) Old electronic component storage board; (b) New electronic component storage board	40
3.31	Board covers are slid to enclose the storage board	40
3.32	Base storage compartment filled with stored components	41
3.33	Isometric view of the mobility subsystem	42
3.34	Assembly of manipulation components in Solidworks	42
3.35	The overall prototype design of the latex cup robot collector	43
3.36	Free body diagram for robot on the inclined surface	45
3.37	Forces acting perpendicular to point O on the main arm	48
3.38	3 separated parts of gripper set	49
3.39	Split lines for different loads exerted on robot platform (top & bottom)	52
3.40	Free body diagram for the robotic arm	53
3.41	Forces exerted by the robotic arm on the robot platform	55
3.42	Fixture applied on the bank of the robot platform	55
3.43	Static analysis settings for robotic arm in Solidworks	56
3.44	Free body diagram of left topple and back topple	59
3.45	Uneven track built for Motion Study in Solidworks	60
3.46	Motor feature setting for motion study	60

3.47	Compression test conducted on the spring and shock damper	61
3.48	Graph of spring constant calculation for front spring	62
3.49	Laptop stand for the topple angle test	64
3.50	Experiment floor setup	65
3.51	Latex cups at 3 different heights on “rubber tree”	65
3.52	Experiment floor setup for mobility test	66
3.53	The project’s overall flowchart	67
3.54	FYP 1 Gantt Chart	69
3.55	FYP 2 Gantt Chart	70
4.1	Prototype of the Latex Cup Collector Robot (Isometric view)	72
4.2	Four different views of the prototype	72
4.3	Stress plot for the robot platform	74
4.4	Displacement plot for the robot platform	74
4.5	Deformation happens on the printed robot platform	75
4.6	Strain plot for the robot platform	75
4.7	Stress plot for the extended robotic arm	76
4.8	Section view of the gripper part (stress plot)	77
4.9	Displacement plot for the extended robotic arm	77
4.10	Strain plot for the extended robotic arm	78
4.11	Measurement of centre of mass from each direction	79
4.12	Working process for the prototype to collect the latex cups for a cycle	83
4.13	Robotic arm collects latex cup at 160 mm height	85
4.14	Robotic arm collects latex cup at 120 mm height	85

4.15	Robotic arm collects latex cup at 105 mm height	85
4.16	Pitch, yaw, and roll illustration	86
4.17	Pitch, Yaw, and Roll angle ($^{\circ}$) versus time (s) graph for motion study	87
4.18	The prototype passes two barriers on the left and right sides (side view)	88
4.19	The prototype passes two barriers on the left and right sides (front view)	89

LIST OF SYMBOLS / ABBREVIATIONS

a	acceleration of robot, m/s^2
d_n	distance between F_n and point O, where $n = A$ and B , m
F_n	force exerted perpendicular to the point O, where $n = A$ and B , N
F_s	spring force, N
F_y	force acting on Y-direction, N
f_{wheel}	force pushing against the wheel, N
$f_{gravity}$	force pulling robot down incline due to gravity, N
g	gravity, $\text{m}\cdot\text{s}^{-2}$
H_{it}	height of inner tank, mm
$I_{part 1 and 2}$	mass moment of inertia of part 1 and 2, $\text{kg}\cdot\text{m}^2$
$I_{part 3}$	mass moment of inertia of part 3, $\text{kg}\cdot\text{m}^2$
k	spring constant, N/mm
L_0	initial spring length, mm
L_c	compressed spring length, mm
L_{it}	length of inner tank, mm
M_a	moment at point A, $\text{N}\cdot\text{mm}$
m_c	mass of component, kg
m_n	mass of part n , g
m_{robot}	mass of the robot, kg
RPM_{input}	rotational speed required by the motor to drive the differential gear, rev/min
RPM_{output}	output rotational speed required by the rear wheels to drive the robot, rev/min
r	radius of the rear wheel, m
t	time, s
t_a	time for the robot to reach maximum speed from rest, s
U_y	force acting on point U in Y-direction, N , where $U = A, B, C,$ and D
V_{it}	volume of inner tank, mm^3

v_o	initial Speed of the robot, m/s
v_{max}	maximum Speed of the robot, m/s
W_{it}	width of inner tank, mm
W_c	weight of component, N
W_{base}	weight of base, N
W_{arm1}	weight of main arm, N
$W_{Connector}$	weight of connector, N
W_{arm2}	weight of horizontal arm, N
$W_{support}$	weight of gripper support, N
$W_{gripper}$	weight of gripper set, N
X	horizontal distance of centre of mass from the robot side, mm
x	spring stretch or compression, mm
x_{cg}	centre of gravity in x direction relative to a point, mm
x_n	centre of gravity of component n in x direction relative to a point, mm
Y	vertical distance of centre of mass from the floor, mm
y_{cg}	centre of gravity in y direction relative to a point, mm
y_n	centre of gravity of component n in y direction relative to a point, mm
z_{cg}	centre of gravity in z direction relative to a point, mm
z_n	centre of gravity of component n in z direction relative to a point, mm
α	angular acceleration, rad/s ²
δ_o	Steering angle of outer wheel, °
δ_i	Steering angle of inner wheel, °
θ_{topple}	topple angle, °
θ_{slope}	maximum slope incline to travel, °
τ	torque, N·m
τ_{input}	torque required by the motor to drive the differential gear, N·m
τ_{output}	output torque required by the rear wheels to drive the robot, N·m
$\tau_{part 1 \& 2}$	torque required for part 1 and part 2, N·m
$\tau_{part 3}$	torque required for part 3, N·m
ω	angular velocity, rad/s

AI	Artificial Intelligent
CAD	Computer aided design
DC	Direct-current
DoF	Degree of Freedom
FEA	Finite Element Analysis
GR	Gear ratio
IE	Industrial Engineering
IoT	Internet of Things
PA	Precision Agriculture
PLA	Polylactic Acid
RPM	Revolution per minute
STL	Stereolithography
3D	Three-dimensional
4WD	Four-wheels-drive

CHAPTER 1

INTRODUCTION

1.1 Background

As defined by Cambridge University Press (1999), robot is "a machine controlled by a computer that is used to perform jobs automatically". Besides, according to Logsdon (2000, cited in Robot Institute of America, n.d.), robot is defined as a reprogrammable manipulator created to perform a variety of tasks through changeable moves without changing its basic structure. For instance, a robot conducts part changing by itself with instructions given while the machine still needs operation by humans.

Robots can easily be divided into two categories, which are fixed robots and mobile robots. Fixed robots are those attached to a fixed position and use robotic manipulators to conduct tasks, while mobile robots are those created with single or multiple wheels, tracks, or legs to travel around, such as self-driving cars. Furthermore, robots can also be classified into two other categories, which are industrial robots and service robots. Industrial robots are robots that work in industries for production purposes, while service robots are robots that assist humans in their tasks outside the industrial field. For the latex cup robot collector in this project, it is the agricultural robot that is classified under "mobile" and "service" robots.

Agricultural robots are one of the technologies grouped under Precision Agriculture (PA). As defined by Lowenberg-DeBoer and Erickson (2019), PA is the use of technology as a means of improving agricultural operations. There are three

areas associated with PA, which are IoT, AI, and robotics. These three areas can be implemented either alone or together. Oliveira et al. (2021) claimed that robotics was the main choice for all previous researchers to improve agricultural activities. This is because robotics could carry out repetitive responsibilities with excessive attention and with much less error. Therefore, it verified the use of robots in the agriculture field that boost productivity and enhance quality while reducing labour costs and operating time (Pant et al., 2019).

In addition, due to the COVID-19 outbreak that spread over the world, several forms of restrictions on social and economic activities were imposed (Oliveira et al., 2021). This strongly affects the agricultural sector because lots of workers are needed for activities like planting, sowing, and harvesting. According to Oliveira et al. (2021) too, it is estimated that there will be a 28.94% increment in the world's population by the end of 2050. This eventually increases the usage of natural elements to produce various products for mankind to fulfil their needs nowadays. For instance, rubber is largely harvested to produce products such as tires, gloves, mattresses, and paintings. Thus, the investment of agricultural robots in rubber plantations is significantly important as it can bring many benefits to the community.

1.2 Problem Statements

Southeast Asian countries are the most significant rubber producers today. 93% of the world's natural rubber production is accounted for in Asia, and Malaysia is one of the largest producers (Business Wire, 2020). According to the Malaysian Rubber Council, MRC (2021), total world rubber production and rubber consumption resulted in a huge 7.30% and 10.41% rise, respectively, in the year 2021 as compared to the year 2020. However, in Malaysia, there was a 3.92% decline in rubber production and a 4.74% climb in rubber consumption from the years 2020 to 2021, as shown in Figure 1.1 (MRC, 2021).



Figure 1.1: Malaysia's Rubber Production and Consumption (in thousand tonnes), 2017-2021 (Source: MRC 2021 cited in IRSG, 2021)

Based on Figure 1.1, rubber consumption in Malaysia for the last five years was always higher than rubber production, while production itself fell throughout these five years, despite Malaysia being one of the world's largest rubber producers. At the bottom of it, what are the factors that led to low rubber production in Malaysia?

The main factor is the reduction of the labour force in the rubber plantations. This is mostly because of the health issues of workers. Musculoskeletal symptoms are a significant health issue posed among rubber workers. They always lower their backs or turn their heads up to tap the trees (Doi, Yusuff and Leman, 2014). Furthermore, because the rubber trees are always located on rough and uneven ground, rubber workers find it difficult to perform tasks and must expend a lot of energy to balance their bodies on the ground (Doi, Yusuff, and Leman, 2014). Thus, these health problems cause the workers to reduce their workload and eventually reduce their production. Besides, fewer and fewer people are involved in the rubber plantation industry. "Younger people these days feel it is not worth it to tap the rubber," said Ab Manap Minhat, a rubber worker, in an interview with Channel News Asia, CNA (Tan, 2020). This is because rubber workers earn lower salaries and tend to be involved in much more comfortable and well-paid jobs. If we rely solely on older workers in the rubber plantation, efficiency and productivity will suffer.

Moreover, latex surgical gloves and other latex medical products are in high demand in Malaysia due to the COVID-19 outbreak (Tan, 2020). However, Malaysia, a latex producer, has to import rubber from other countries to catch up with the shortage in local production because the total consumption is larger than the local production, said Zairossani, the Malaysian Rubber Board's Director to CNA (Tan, 2020). This is due to the preferred latex harvesting mode in Malaysia. Rubber workers like to collect the latex in cup lump form, which has already been hardened by overnight coagulation, because cup lump production is easier and offers more convenience in terms of collection (The Edge Markets, 2020). Workers can leave the latex overnight instead of collecting them after just a few hours of tapping. However, gloves and other latex products demand liquid latex. So, the downstream manufacturers have to import liquid latex from other countries.

1.3 Aims and Objectives

The aim of this project is to design and develop a latex cup collector robot. The objectives are shown as following:

- i) To design a mobile robot that can move on different terrain surfaces with a 4 Degree of Freedom (DoF) movement robotic arm to collect the latex cup at different heights.
- ii) To analyse and evaluate the robot design by using Finite Element Analysis (FEA) and Motion Study Analysis by using Solidworks.
- iii) To develop and fabricate a workable prototype for the designed robot by using a 3-Dimensional (3D) printer.

1.4 Scope of Project

The scope of this project was to design a robot that fulfils high flexibility and high stability criteria. So, a latex cup collector robot was studied, designed, and developed. Then, the robot prototype was tested on uneven terrain to test its availability. Besides, it was also able to conduct the pick, pour, and place tasks repeatedly.

However, the cost of materials and the prototype size were the limitations of this study. Due to the limited budget of this project, all the decisions were very prudent. Furthermore, because of the size restriction of 200 mm, which can only be printed by the Ender 3 3D printer, many of the design means cannot be made due to the small dimensions of components that are not available on the market. As a result, all design parameters were carefully considered so that the project's budget would not be exceeded.

1.5 Outline of Report

Chapter 1 presents the background of the agricultural robot, the problem statement, aim and objective, and the scope of the project. Next, Chapter 2 conducts literature reviews on the latex properties and the overview of agricultural robots to grab some knowledge and ideas from previous works and papers that can contribute to the design and fabrication of this latex cup robot collector. Chapter 3 then discusses prototype design methodology and methods for conducting simulations and tests on specific parts or the entire prototype to gain insight into the mechanical effects on the prototype. A flowchart and Gantt charts are also attached in Chapter 3 to track the project's progress. In Chapter 4, results from the simulations and tests are shown and discussed, while in Chapter 5, the project is concluded, and some recommendations are made for future study.

CHAPTER 2

LITERATURE REVIEW

2.1 Introduction to Latex

Latex is a white, milky sap that can be found beneath the bark of the rubber tree. There is always a misunderstanding that latex and natural rubber are the same thing. It can be briefly explained as latex is a raw material while natural rubber is the product of latex through coagulation or industry processes. Latex has the potential to protect plants from injury and insects (Liné, 2020). Besides, there are about 10% of all the plants in the world that produce latex. But for commercial use, latex is frequently and exclusively harvested from a tree primitive to South America, "Hevea brasiliensis" (Encyclopaedia Britannica, n.d.).

There are two significant steps to harvest latex from rubber trees in the plantation, which are the tapping process and the collecting process. For the tapping process, the bark of a rubber tree is cut, obtaining a deepened channel by using a sharp tool called a gouge. After that, the latex is allowed to flow along the channel and finally drops into the latex cup tied below the channel through the gutter (Figure 2.1). The latex is dropped for 1 to 3 hours before the collection process (AZO Materials, 2006). This is due to the quick coagulation of latex and must be collected from cups before it coagulates (Liné, 2020). Latex is then poured and accumulated in a large tank by many trees during the collecting process. At this stage, the movement of labour throughout the collecting process will lead to the stability deterioration of latex in the tank. Bacterial contamination in the tank will further exacerbate this reaction (de Livonnière,

1993). Thus, chemicals like ammonia will be added to the tank to slow down the reaction.

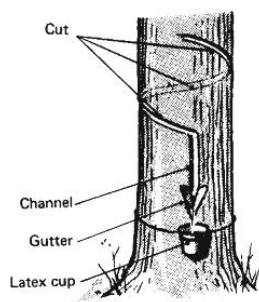


Figure 2.1: The rubber tree tapping process (Source: FAO, 1977)

2.2 Agricultural Robot in Harvesting Process

Agricultural robots can be grouped into different types based on various agricultural processes. These processes included land preparation before planting, sowing and planting, plant treatment, harvesting, and yield estimation and phenotyping (Oliveira et al., 2021). There are also robots designed for livestock maintenance purposes (Manikandan and Srinivasan, 2014). This section will focus on the harvesting robot since the latex cup collecting process in the project is also classified as a harvesting process.

In Japan, the harvesting process represents around 25% of the whole agriculture work (Hayashi et al., 2014), while in China, expensive cotton harvesters use only three months to harvest, while the other time is stored under shed (Fue et al., 2020). These statements indicate that harvesting activity requires a lot of time and is cost ineffective. But on the other hand, the labour cost in Australia's agriculture sector only accounts for 20%–30% of the total production cost (Department of Agriculture, 2014). This is because of the higher level of robotics and automation implemented in Australia's agriculture field (Oliveira et al., 2021). Therefore, due to this, several research projects that use agricultural robots to conduct harvesting processes have been carried out. For instance, strawberry harvesting robots (Ge, Xiong, and Tenorio, 2019),

lettuce harvesting robots (Birrell et al., 2020), and coconut harvesting robots (Megalingam et al., 2020).

2.3 Challenges faced to Introduce Agricultural Robot

Many research projects done on agricultural robotics in the last 30 years never reached their implementation stage (Bechar and Vigneault, 2016). The main reason is that agricultural processes confront a complicated, unstructured, and dynamic environment (Pant et al., 2019). Therefore, it is challenging to introduce agriculture robots because they need to be capable of moving in the rough and uneven agriculture environment (Canning, Edwards, and Anderson, 2004). Besides, most of the agricultural processes are held outdoors, where extreme and hazardous weather will largely affect the robot's performance, such as the sensor's sensitivity (Yaghoubi et al., 2013). This will eventually lead to the malfunction of the robot and result in another challenge for the agricultural robot, which is cost.

Starting from the development stage, the development cost is one of the factors considered. In the past, the excessive cost of the developed system was one of the main reasons that agricultural robots could not reach the implementation stage (Bechar and Vigneault, 2016). Despite robots' successfully stepping into the commercial stage, the repair and maintenance costs are also expensive (Fue et al., 2020). Repairing periods per breakdown will lead to a reduction in operation efficiency because agricultural robots are complicated to repair and take time (Fue et al., 2020). Thus, farmers will rarely choose to implement robots in the agriculture sector because of the excessive cost of repair and maintenance. They also do not see the break-even profit from this revolution (Marinoudi et al., 2019).

Furthermore, agricultural robots are not capable of operating in ill-defined, unknown, unpredictable events (Bechar and Vigneault, 2016). It is challenging to deal with how to use a human approach to address distinct scenarios when designing an autonomous agricultural robot (Ng and Trivedi, 1998). Besides, the diversity of agricultural processes complicates the generalisation of automation (Pant et al., 2019).

For example, driving a robot from tree to tree and detecting, grasping, and detaching fruits requires a lot of algorithms and sensor-motor control formulations (Ceres et al., 1998). With existing knowledge and technologies, robots will lead to production inefficiencies that include long cycle times and low detection rates (Zhao et al., 2016). Thus, further development of advanced technologies should be needed to deal with complicated and unpredictable events (Bechar and Vigneault, 2016).

2.4 Components of Agricultural Robot

Agricultural robots are built to perform their "main task," such as weeding and harvesting (Pant et al., 2019). An agricultural robot has to be capable of performing several "supporting tasks" in order to perform the main task, (Bechar and Vigneault, 2016). For instance, the main task of a harvesting robot is harvesting, so its supporting tasks should be localization, navigation, object detection, and picking operations. Sub-systems are used to execute forces or signals to perform "supporting tasks" and also "main tasks" (Bechar and Vigneault, 2016). Information flows continuously between the systems, controlling the main and supporting tasks results in the effective working of an agricultural robot system, as shown in Figure 2.2 below (Pant et al., 2019). Besides, agricultural robots rely solely on four main components, which are sensing, planning, mobility, and manipulation, to perform tasks (Fue et al., 2020).

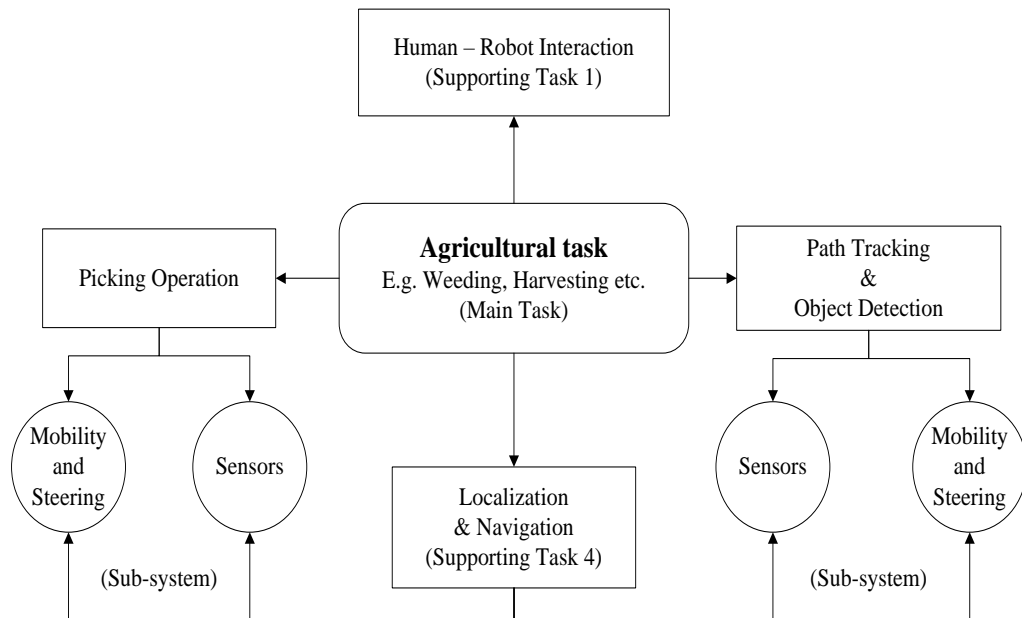


Figure 2.2: Structure of Robot System to Perform Agricultural Task (Source: Pant et al., 2019)

2.4.1 Sensing

Sensing is the perception of the surroundings and their occupied items, which can permit or prevent the operation of the robot (Fue et al., 2020). It is important in agricultural robotic systems because robots need to detect environmental characteristics such as paths, obstacles, targets, and self-position to support decision-making, operations, and other robots' performance (Bechar and Vigneault, 2016). In a robot system, sensors can be divided into internal and external sensors (Bechar and Vigneault, 2016). Internal sensors measure the robot's inner nation and they're used to some degree to determine its position, speed, and acceleration. For example, gyroscopes measure the rotational acceleration. On the other hand, external sensors are sensors that adhere outside the body to gather or collect information from the environment in order to receive information and execute supporting tasks and main tasks. For example, soil sensors, temperature sensors, vision sensors, GPS sensors, and crop sensors.

2.4.2 Planning

Path planning is considered one of the most required “supporting tasks” for agricultural robots (Bochtis, Sørensen, and Busato, 2014). This is because it is responsible for finding the optimal track for the robot to move from a source point to its destination point while avoiding the obstacles along the path (Bhattacharya and Gavrilova, 2008). This path planning is made possible by the cooperation of sub-systems and supporting tasks. For example, the sensor senses the environment and transfers the information to the steering to turn the wheels for navigation and path planning. In harvesting, path planning depends on the crops, manipulators, and end-effectors. Path planning will be expensive when the plants have to be harvested without destroying them and when the manipulators’ DoF increases (Fue et al., 2020).

2.4.3 Mobility

As a mobile agricultural robot, mobility and steering sub-systems are significant to provide the movement ability of the robot for navigation, moving from one place to another to conduct its task. According to Pant et al. (2019), ground contact is a crucial parameter for agriculture robots because they need to operate in an unstructured environment such as uneven terrain to prevent any incidents during operation. There are several choices of mobility used for robots in the agriculture sector, which consist of legs, wheels, wings, rail tracks, or drones. Furthermore, one of the important aspects of the agricultural robot's ability to overcome unstructured environments is the suspension system (Pastor et al., 2018). It is mostly used for wheeled robots due to their constant contact with the ground.

2.4.4 Manipulation

A manipulator is mostly an arm-type electromechanical robotic gadget that is executed in a confined space and completes the required task by using a tool called an end-

effector attached at the end (Pant et al., 2019). In the industrial sector, robotic arm manipulators are common. However, it is not suitable for use for agricultural purposes due to its high cost, high power consumption, and heavy weight (Bloch, Bechar, and Degani, 2017). A manipulator for the agricultural domain should be simple and basic (Bechar and Vigneault, 2016) to avoid injury to nearby crops or stems during harvesting. Besides, the DoF of the manipulators can be designed based on the needs of the operation. However, although an increase in DoF improves the flexibility, it also results in a heavier manipulator and a slower response time (Kondo and Ting, 1998).

According to Monta, Kondo, and Ting (1998), end effectors are significant devices in the development of agricultural robots because they grasp the crops directly and can potentially influence the market value of the product. End-effectors have different types based on the tasks they conduct. Impactive end-effectors are used for grasping purposes, ingressive end-effectors are used for penetrating tasks, and attractive end-effectors use external force to attract objects like suction, while contiguous end-effectors directly adhere to the object (Fue et al., 2020).

2.5 Design concepts

In this subchapter, various design concepts are compared and contrasted for two of the agricultural robot's components that are discussed in Chapter 2.4 above: mobility and manipulation. Sensing and planning components will not be discussed here as this project mainly focuses on the mechanical part of the latex cup robot collector. After that, the most suitable design concept for each component will be chosen as the final design of the prototype in the next chapter.

2.5.1 Design concepts for mobility

The mobility of a robot can be further categorised into four subfunctions, which are locomotion, transmission, steering, and suspension. These four subfunctions carry out different actions to form a complete mobility subsystem.

2.5.1.1 Locomotion

For agricultural robots, there are three common locomotion used to cope with the agricultural environment, which are legs, wheels, and treads. For leg locomotion, it is advantageous to be used in the agriculture field due to its flexible movement towards the high occlusion of obstacles (Fue et al., 2020). Besides, legged robots can achieve balance to overcome slopes by adjusting their posture (Silva and Machado, 2011). This can be observed in Zhang et al.'s 2019 study that studied the goat's head movement while walking on different slopes. However, the result showed that as the slope increased, the goat's head (which represents the robot platform) would suddenly fluctuate to achieve balance. The fluctuation will gradually increase when the slope increases. This is not ideal for robots that must transport liquid products, such as the robot in this project. Besides, Wickramanayake (2020) in his study also stated several disadvantages for leg locomotion: being cost-ineffective (requiring complex sensors and motors to operate; regular maintenance is needed to provide precision) and navigating at a slow pace. Figure 2.3 below shows an example of a legged robot.



Figure 2.3: Example of leg locomotion system (Source: Oliveira et al., 2021)

For wheel locomotion, speed performance is the key advantage to be considered in agricultural robots. According to research done by Oliveira et al. (2021), most agricultural robots use wheels, especially four-wheel-drive (4WD), as their locomotion systems. This is mainly because its fast speed of mobility can reduce the time and increase the harvest productivity at low power consumption. However, wheeled robots could be strongly affected by unstructured terrain (Oliveira et al., 2021). This can be demonstrated by the fact that many previous researchers were working to overcome these issues. For example, Nakajima (2011) separated the rear wheels and front wheels by two independent moving axles that could be turned vertically when confronted with obstacles in his robot, RT Mover (see Figure 2.4). Besides, Kim, Jeon, and Yang (2017) proposed a six-wheel transformable mobile robot that can transform in terms of the link and the wheels to encounter different types of terrain (refer Figure 2.5). Thus, wheel robots can perform greatly at low cost, high speed, and low power consumption with the help of external mechanisms such as steering and suspension.

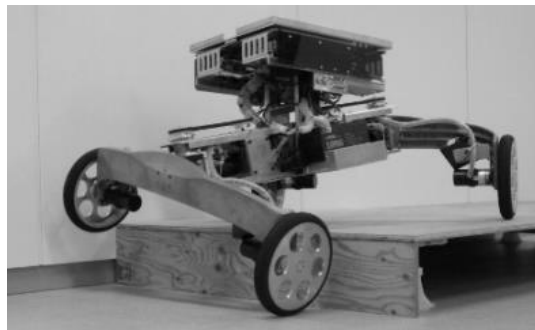


Figure 2.4: RT Mover (source: Nakajima, 2011)

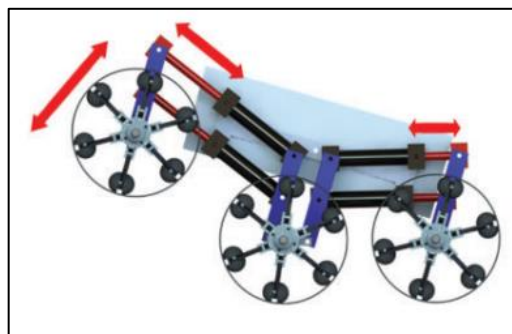


Figure 2.5: Transformable mobile robot with six wheels (Source: Kim, Jeon, and Yang, 2017)

While for track locomotion, it is well suited to travelling on soft terrain such as sand or mud surfaces and overcoming obstacles because tracks have a large ground contact surface to the ground (Bruzzone and Quaglia, 2012). However, due to the lateral track profile, this locomotion travels slowly and consumes more energy, which at the same time affects the mechanical efficiency (Bruzzone and Quaglia, 2012). Besides, large vibrations that are produced by the motor rotation will affect the robot platform and may lead to the spoilage of the components onboard (Wickramanayake, 2020).

2.5.1.2 Transmission

Three means, which are: differential drive, direct drive, and chain drive, have been proposed for the robot's transmission.

Differential drive has a feature that can increase the feasibility of dealing with rotation speed offsets between wheels while turning vehicles, as well as deal with changes in ground-wheel contact surface and friction effects on each side of the wheels. (DeSantis, 1995). This transmission system is commonly used in vehicles on the road because it can be used at sharp turns that require the outer wheel to rotate much more than the inner wheel. Researchers such as Kitagawa et al. (2009) and Ueno et al. (2010) studied the use of differential drive systems. In their studies, a differential gearing system was used to improve the operation ratio of the motors of each wheel to produce a resultant rotation so that each wheel could turn at a different steering angle and different rotation speed to provide stable robot turning. However, two motors were applied to each wheel in these studies to produce the driving and steering functions, respectively. It is much more expensive as compared to the differential drive of the vehicle on the road. Thus, the concept of vehicle differential drive is more favourable if budget is the limitation of the project.

According to Hoogewijs (2020), direct drive provides a more efficient way to the transmission system. This is because all the motor power would be transmitted directly to the locomotion system by the direct gear to two connected gears, and lastly

to the wheels. This is good when the robot is moving in a straight line. But if turning is required, the inner wheels of the robot will encounter slipping problems, or the robot will be turned in an unstable state due to the different path lengths for inner and outer wheels.

Chain drive transmission, on the other hand, is commonly used on bicycles and motorcycles. It is advantageous to perform in severe environments such as dirt, high temperatures, and moisture (Hoogewijs, 2020). Besides, it is also able to provide high efficiency in transmitting energy with about 98% efficiency. This is because slip would not occur as it occurs in belt and rope drive (Anjum et al., 2012). Teeth on the sprocket mate perfectly with the chain holes to prevent slippage. However, the cost of implementing chain transmission is higher and it needs to be serviced frequently, such as lubricating the chain to slow the chain's wear.

2.5.1.3 Steering

The Ackerman mechanism is the first choice for the steering subfunction. In this steering system, a steering arm (also known as tie-rod linkages) is used to turn both the front wheels synchronously. This mechanism causes the turning radii of both wheels to be different, which means that the inner wheel experiences a greater steering angle than the outside wheel. By this, the slipping effect will be reduced, and this is significant when the robot travels at high speed (Hrbacek, Ripel and Krejsa, 2010). There is a principle that should be satisfied to perform Ackermann steering. The inner ends of both wheels are designed to pivot. Both of the pivot ends are where the steering arm is attached. Besides, the angle of both pivots should be aligned with the Ackermann axis and the centre of the rear axle so that the wheels can intersect at the centre of rotation when the wheels turn (refer Figure 2.6). According to Hrbacek, Ripel and Krejsa (2010) too, the use of differential drive systems together with Ackermann steering promotes the greatest efficiency and advantages, such as high speeds.

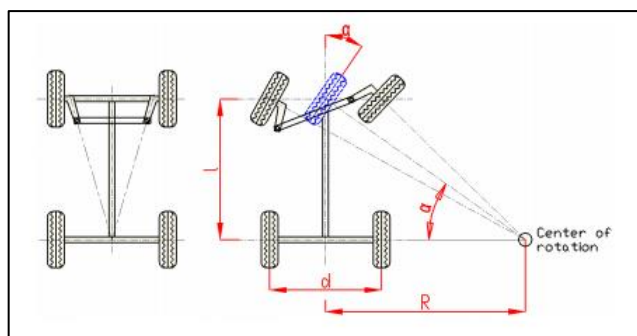


Figure 2.6: Ackermann steering principle (Anon., n.d.)

For 4-wheel steering, it is an extended version of Ackerman steering. The rear wheels also steer or turn in different directions and at different angles than the front wheels to ensure understeer and oversteer (Sundar, Sudarsanan and Krishnan, 2018). Besides, a 4-wheel steering system can also improve steering response and increase stability (Sundar, Sudarsanan and Krishnan, 2018). However, the disadvantages of 4-wheel steering are that too many motors are required. For instance, eight motors are needed when the robot implements 4WD and 4-wheel steering together. This not only increases the weight of the robot, but it also increases its power consumption. Besides, the complexity of control system algorithms also increases since each motor has its own logic action to be performed.

Moreover, skid steering is a steering system without the turning of the wheels in left and right directions. Its steering mechanism is based on the wheels slipping and controlling the rotating velocities and direction of each wheel (see Figure 2.7). The advantages of skid steering are that it has high manoeuvrability despite having a simple structure (Wang et al., 2015). Besides, it is adaptable to many types of terrain as it has good mobility. However, due to the simple structure, it should have to be developed with complicated kinematic and dynamic formulations so that it can execute the movement accurately (Wang et al., 2015). Moreover, due to consistent slipping of the wheels, this steering system is said to be energy-consuming, and the wheels spoil faster (Kozłowski and Pazderski, 2004).

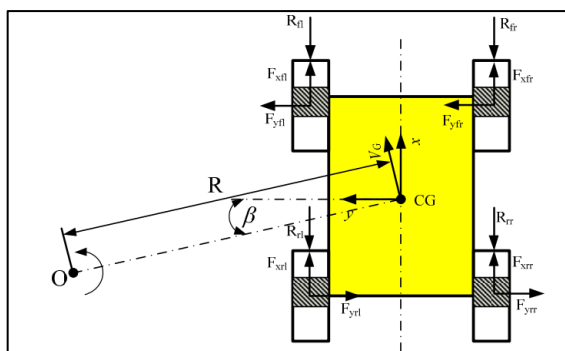


Figure 2.7: Different rotation velocities of the four wheels produce the resultant turning angle for the overall robot. (Source: Wang et al., 2015)

2.5.1.4 Suspension

Spring, double wishbone, and Roker Bogie mechanisms are proposed for the suspension subfunction. The spring in the suspension system is mostly embodied in the coil shape. The characteristic of a spring is that it has good elasticity, which allows it to deform when external forces are applied and return to its initial position when the forces diminish (AlSahlani, Khashan and Khaleel, 2018). Besides, the suspension system in a robot can also ensure the robot's reliability by protecting the internal mechanical and electrical components from shocks and vibration. In a study done by Roh et al. (2013), they implemented a novel suspension system called "multi-layered suspension" that is a combination of springs and dampers and is not powered by any actuator. With the combination of both springs, the previous problems such as being unable to restore to the initial position and overturning incidents due to acceleration or deceleration have been solved (Roh et al., 2013). Thus, this suspension system is suitable to be used in this project as collisions and sudden stops are predicted to be common.

While for double wishbone suspension, there are two parallel bars that connect the wheels to the robot's chassis. It is used with the support of a shock damper to provide the suspension effect. Thus, it ensures large vertical movement of wheels (Hoogewijs, 2020) while promoting higher stability for the chassis when encountering unstructured environments. Fauroux and Bouzgarrou (2011) have conducted a study

on this matter to test the availability of double wishbones for the speed of the robot and the height of the obstacles. In their studies, they concluded that double wishbone suspension has a stability limit. The robot can only use high speed to cross low obstacles and use low speed to cross high obstacles. The robot will tip-over if there is low speed on high obstacles and high speed on low obstacles. Thus, they also suggested that this stability limit can be controlled by observing the obstacle height using sensors before crossing the obstacles to prevent the tip-over incident.

On the other hand, Roker Bogie is a springless suspension system that requires six wheels. The "rocker" represents the main driving wheels, while the "bogie" acts as the idler to help to distribute the load of the robot body and even stabilise the robot. The dimension of the rocker-bogie is determined by using the Pythagorean theorems and, normally, both rocker and bogie linkages have an angle of 90° (refer Figure 2.8). Besides, both sides of the rocker linkage are connected to each other by a rod called a differential arm. With this design, it ensures all the wheels remain in contact with the surface when climbing over hard and rough terrain (Saraiya, 2020). Besides, because of bogie wheels, the pressure on the ground will be equilibrated and distributed to cause less harm to the soft soil terrain (Saraiya, 2020).

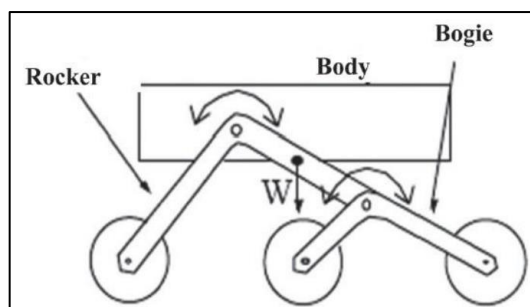


Figure 2.8: Rocker-bogie suspension system (Source: Yadav, Bhardwaj and Bhardwaj, 2015)

2.5.2 Design concepts for manipulation

Manipulation of a robot can be further categorised into two subfunctions, which are manipulator and end-effector. A manipulator is used as a guide for the end-effector to

reach the object or target and conduct its task. Thus, the design concepts for these two should be interrelated in order to perform precisely.

2.5.2.1 Manipulator

There are two choices proposed for manipulators, which are pneumatic, and motor driven. For pneumatic manipulators, a pneumatic actuator is used to move the manipulator by pumping and compressing the air pressure inside the actuator. It promotes high accuracy and high repeatability (Gonzalez, 2015). However, due to pressure losses and air compression, the efficiency of the pneumatic manipulator will be affected (Gonzalez, 2015).

On the other hand, motor-driven manipulators mostly use servo motors as the driving equipment. As compared to pneumatic manipulators, electric-working devices offer higher precision-control positioning and can perform work quicker, smoother, and more efficiently (Gonzalez, 2015). Besides, it can also be programmed to control the velocity, torque, position, and applied force (Gonzalez, 2015).

2.5.2.2 End Effector

The end effector chosen should have the gripping function to collect the latex cup from the tree. Thus, suction and grippers are proposed for this subfunction. For suction end effectors, the advantage is the ability to handle various shapes of targets (Universal Robots, 2020). However, the air flow must be uninterrupted when holding the items which then increases the power and electric consumption (Universal Robots, 2020). Besides, the efficiency will also be affected due to the harsh conditions (Universal Robots, 2020).

For the gripper end effector, it consists of two moveable fingers to perform the gripping process (Lundström, 1974). It is advantageous in speed when finger opening

and closing (Universal Robots, 2020). Sometimes, three fingers are the best choice when handling round and cylindrical objects.

2.5.3 Design concepts for storage tank

The storage tank acts as a temporary storage to store the liquid latex during the harvesting process by the robot. Looking into the rectangular storage tank, the key properties are that it promotes high organizing, stacking, and shipping efficiencies (Quora.com, n.d.). It can be used to maximise the space and fit better when space is an issue. It also provides a larger volume of storage as compared to the cylindrical tank. Besides, a rectangular tank will provide greater cost effectiveness because fabricating planar shapes is much cheaper than curved surfaces (Quora.com, n.d.).

On the other hand, the cylindrical tank also has its advantages. According to Hegde, Yogesh and Chawhan (2018), a cylindrical tank can withstand higher principal stress and provide greater hoop tension as compared to a rectangular tank. Cylindrical tanks can also better minimise the surge effect of liquid inside the tank to cope with the problem of inertia during transportation (Wacme Pty Ltd, 2021). Cylindrical tanks also possess a low centre of gravity, making them more stable, and there is no structural weak point for cylindrical tanks as there is no corner to accumulate pressure (Wacme Pty Ltd, 2021).

CHAPTER 3

METHODOLOGY

3.1 Chosen Design

After overviewing all the possible design concepts that were proposed in the previous chapter 2.5, suitable concepts that fulfilled the scope of study were chosen for building the final prototype design. As a summary, Table 3.1 below shows the chosen means that were used for the prototype design. After that, it is time to start the prototype design using Solidworks software.

Table 3.1: Chosen means of each subfunction for the design

Subfunction	Means
Locomotion	Wheel
Transmission	Differential
Steering	Ackerman
Suspension	Double Wishbone + spring
Manipulator	Motor Driven
End Effector	Gripper
Storage Tank	Rectangular

3.2 Prototype Design and Material Selection

This prototype was designed at a ratio of 1: 10 to the actual product. All the components, such as the motor, differential gear box, and shock damper, were designed to the scale that can be found and available on the market. So, subchapter 3.3 below demonstrates the chosen design for each subfunction in detail.

3.2.1 PLA Material in Solidworks Software

As the final prototype design will be fabricated using a 3D printer, the 3D printing filament material was applied to most of the parts in the prototype. In this project, the filament used to fabricate the model is polylactic acid (PLA) plastic. However, this PLA plastic was not available in the Solidworks software. So, its properties were manually input into the software and applied to the parts for future simulation and analysis use. Properties such as density, tensile strength, and elastic modulus are determined by Matweb (2020) and are shown in Figure 3.1 below.

Model Type:	Linear Elastic Isotropic	<input type="checkbox"/> Save model type in library
Units:	SI - N/mm ² (MPa)	
Category:	Plastic	
Name:	PLA	
Description:	-	
Source:		
Sustainability:	Undefined	Select...

Property	Value	Units
Elastic Modulus	3800	N/mm ²
Poisson's Ratio	0.36	N/A
Shear Modulus	1287	N/mm ²
Mass Density	1240	kg/m ³
Tensile Strength	60	N/mm ²
Compressive Strength		N/mm ²
Yield Strength	70	N/mm ²
Thermal Expansion Coefficient		/K
Thermal Conductivity		W/(m·K)
Specific Heat	1386	J/(kg·K)
Material Damping Ratio		N/A

Figure 3.1: Material properties of PLA plastic input in Solidworks

3.2.2 Locomotion Design (Wheels)

Wheels were chosen for locomotion because they promote fast travel. The design can be separated into front wheel and rear wheel designs. For agricultural vehicles, the rear wheels are always bigger than the front wheels. This is because big rear wheels need to provide better grip on the ground and also distribute the weight much more evenly as most of the forces are acting at the rear wheel (Sacrewell Farm, 2017), while the smaller front wheel provides the sharper steering angle for the robot (Sacrewell Farm, 2017). Thus, the rear wheel was designed with an outer diameter of 85 mm and a width of 31 mm (refer Figure 3.2), while the front wheel was designed with an outer diameter of 65 mm and a width of 24 mm (refer Figure 3.3).

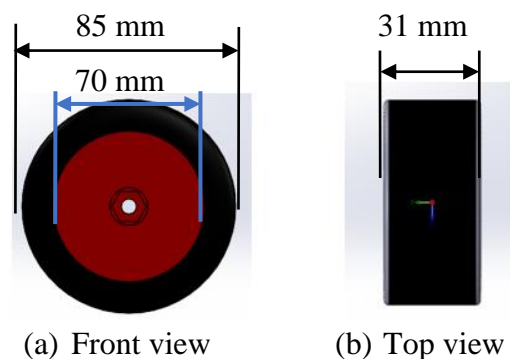


Figure 3.2: Rear wheel design in Solidworks

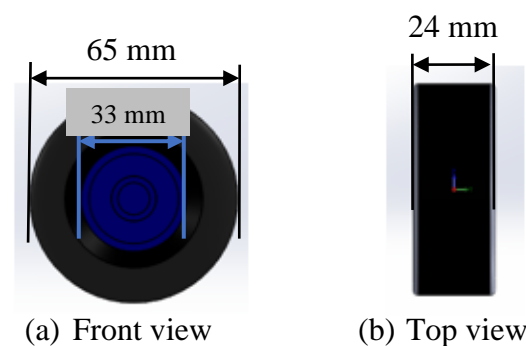


Figure 3.3: Front wheel design in Solidworks

3.2.3 Transmission Design (Differential)

Differential drive was chosen as the transmission system because the robot was driven by just using one motor instead of using an individual motor at each wheel. Besides, the differential effect also adds values to the transmission system when confronting rough and harsh terrain, achieving higher performance.

The key component in differential transmission is the differential gear box. It is a combination of four types of gear that work together to give a flexible and different rotation speed to each side of the rear wheel in different conditions. Figure 3.4 illustrates the differential gear model built in the Solidworks software. However, the dimensions used for the design are not the actual dimensions of the differential gear. This is because of the limitation of Solidworks software to building smaller gears. Besides, it is also difficult to measure the actual product dimensions as it will come in an assembled set. Thus, the differential transmission built here was just to give a picture of the design, and it was also assumed that it did not affect the simulation of the FEA analysis.

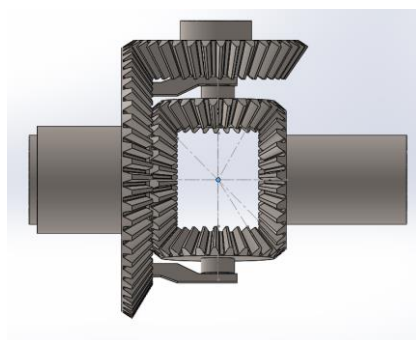


Figure 3.4: Differential gear design in Solidworks

After that, the complete differential gear is covered by the case and mounted with the axles that connect with the rear wheel on each side. Figure 3.5 below shows the Solidworks design of the rear axle with the differential gear chosen for the prototype.

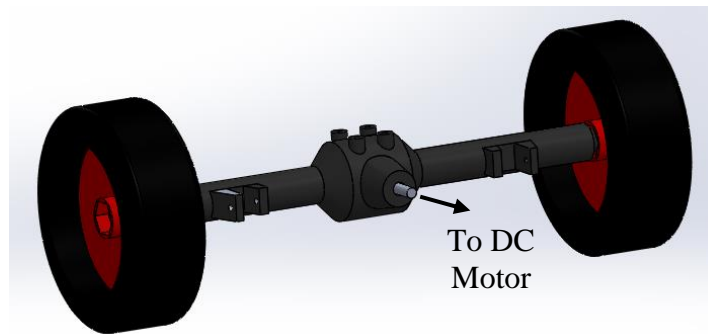


Figure 3.5: Rear axle with differential gear mounted with rear wheels

The rear axle was connected to a direct current (DC) motor that transmits the drive force to the wheels. However, since the DC motor was not at the same level as the rear axle, it means that a straight and fixed driving shaft was not applicable in this case. Thus, the propeller shaft that is commonly used in cars was applied here because it allows torque to be transferred between the components in different positions (Energy Education, 2018). Universal joints were incorporated into this propeller shaft to give it movement allowance between both ends. Figure 3.6 illustrates the universal joint's part, while Figure 3.7 shows the complete differential transmission that transmits power from the DC motor to the wheels.

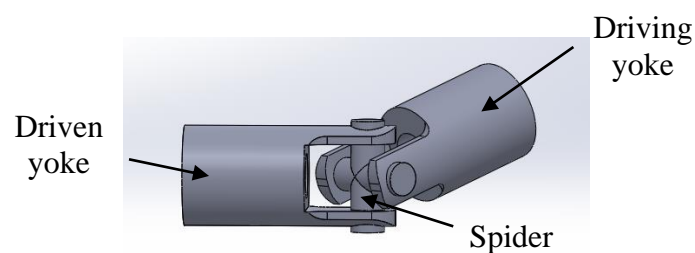


Figure 3.6: Universal joint design in Solidworks

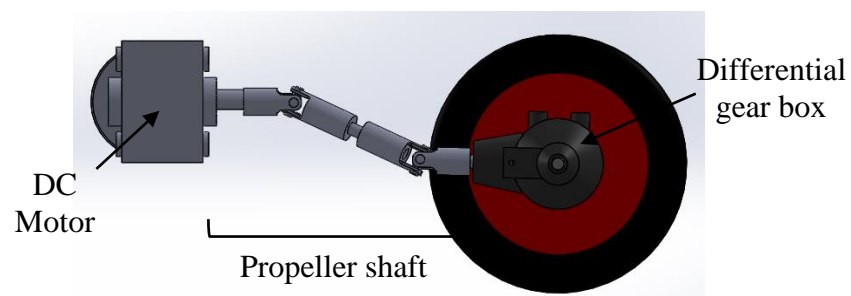


Figure 3.7: Differential transmission design in Solidworks software (Side view)

3.2.4 Suspension Design (Double wishbone and spring)

Double wishbone and spring suspension were both chosen for the suspension system because they can recover from external stimuli. The rear wheel was supported by spring suspension, while the front wheel was supported by a double wishbone. The reason for using different suspension types is that it is not suitable to use double wishbone in the rear wheel part as the wheel axle is all fixed in a straight position. Thus, spring suspension was used as an alternative, even though it is not as good as the double wishbone.

A double wishbone suspension system was applied to the front wheel. Similar to common vehicles, the double wishbone designed for this project also consists of lower and upper wishbone arms, the shock dampers, and the wheel hubs. A pair of shock dampers are used here to absorb the external impact, such as the stones and uneven surface acting on either side. The shock damper had a hole-to-hole length of 100 mm and could be compressed to 75 mm (refer Figure 3.8). Figure 3.9 illustrates how various shock damper conditions affect the double wishbone system.

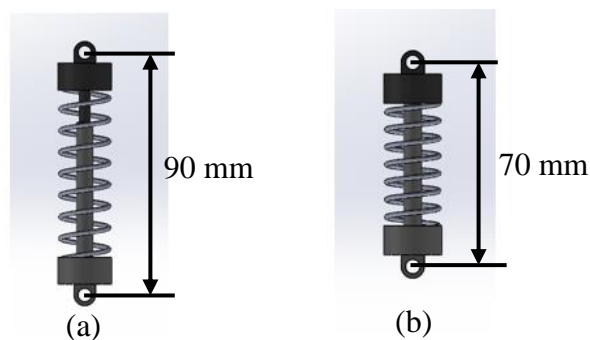


Figure 3.8: Shock damper in (a) uncompressed and (b) compressed states.

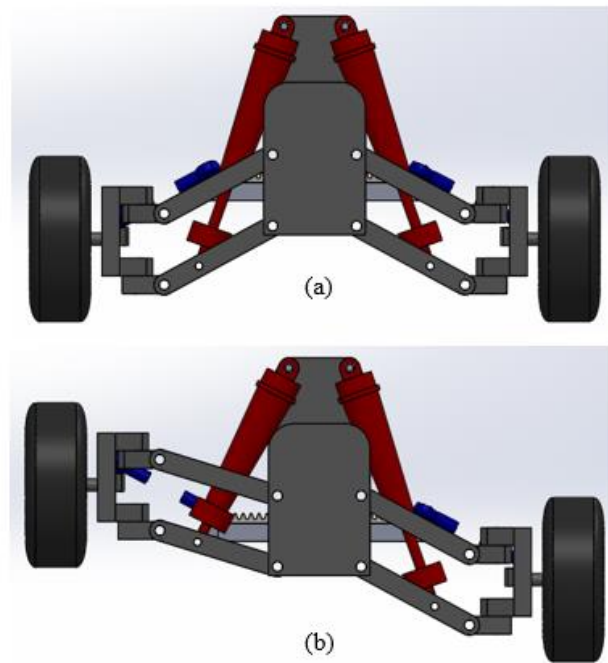


Figure 3.9: Double wishbone suspension system used in the front wheel part. (a) When both sides are in the origin position; (b) When only one shock damper is compressed

For spring suspension, two compressive springs are used. These two springs were located on the spring holders that screw onto the wheel axle, which is 30 mm away from the centre of the wheel on each side. Figure 3.10 illustrates the use of spring suspension in the rear wheel part in Solidworks.

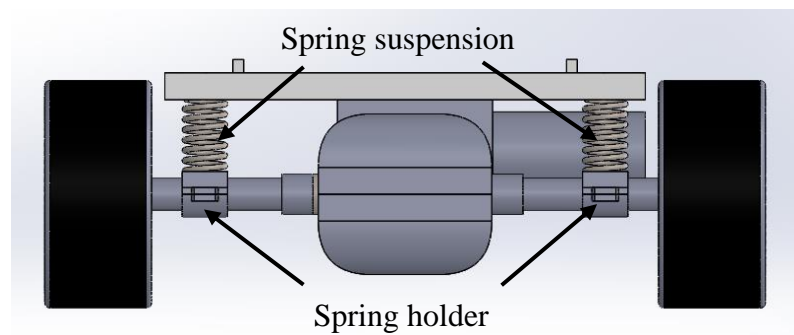


Figure 3.10: Compression spring used in rear wheel part

However, this design seemed to be impossible because there was no support between the robot platform and the rear axle. This will cause the platform to swing randomly and affect the stability of the robot. Thus, the redesign of this part is complete. Instead of connecting the spring solely to the rear axle and base, two identical beams are designed to provide 3-point support between the rear axle and base, with two shock dampers connected to the beams and base, as shown in Figure 3.11.

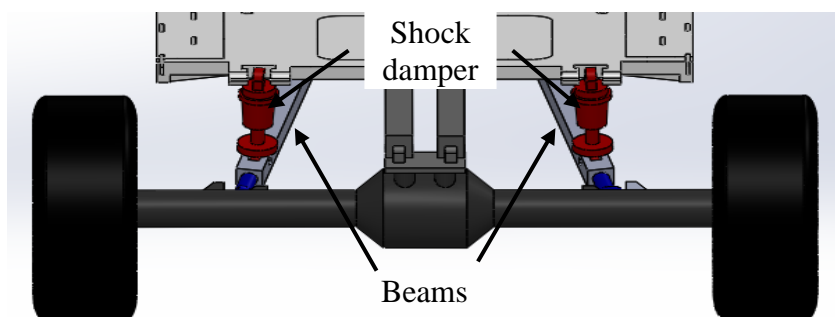


Figure 3.11: Re-design of the spring suspension part (rear)

3.2.5 Steering Design (Ackermann Mechanism)

Furthermore, Ackerman steering was chosen because, as compared to the other two steering mechanisms discussed in Chapter 2.5.1.3, Ackerman requires only one motor to turn both front wheels. Besides, Ackerman can also provide sharper turns, which increases the accuracy in path planning.

For Ackermann's steering design, the two front wheels were turned by a steering bar linked to the steering motor. An extended arm was designed on the wheel hub (refer Figure 3.12) to hold the steering bar, so that two wheels could turn left and right together to perform a turning action.

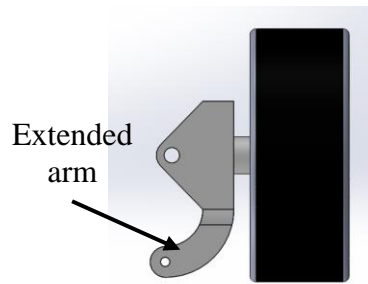


Figure 3.12: Wheel hub design in Solidworks

Due to the suspension system, the wheels would move up and down to absorb the impact and return to their position. Thus, the linkage designed should be able to move freely. Therefore, a ball joint was implemented in this design to encounter this problem. A common ball joint consists of a socket and a ball (see Figure 3.13). It provides pivoting movement for either end when the other end is fixed in position. Thus, two ball joints can be connected with a rod to become a ball joint linkage rod. Figure 3.14 shows how the ball joint linkages were used in the steering system.

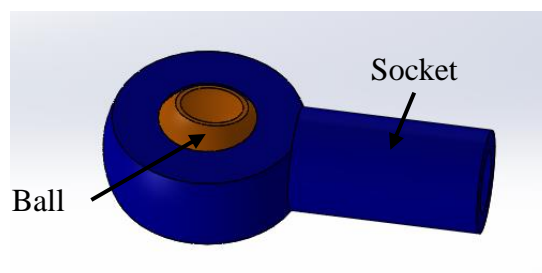


Figure 3.13: Ball joint design in Solidworks

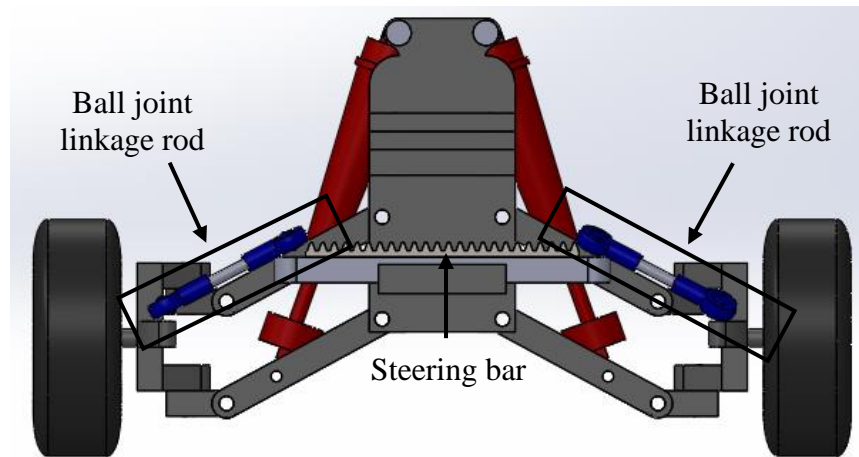


Figure 3.14: Ball joint linkage rods used to connect the steering bar and wheel hubs

Besides, to turn the steering bar, a DC motor was used to perform this task. The DC motor was mounted with a gear. The function of the gear is to transfer the rotational motion to linear motion by grasping the rack teeth of the steering bar, and this is why the steering bar was designed as shown in Figure 3.14 above. For better understanding, Figures 3.15, 3.16, and 3.17 illustrate how the DC motor is used to turn the wheels.

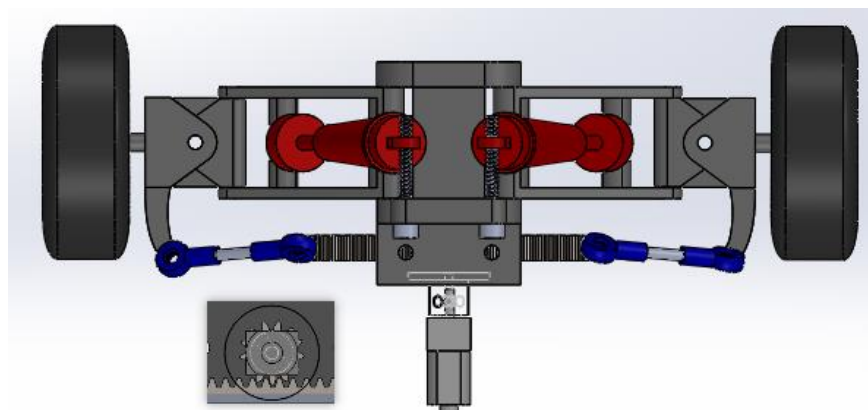


Figure 3.15: The servo motor is set to its default position (wheels are aligned straight)

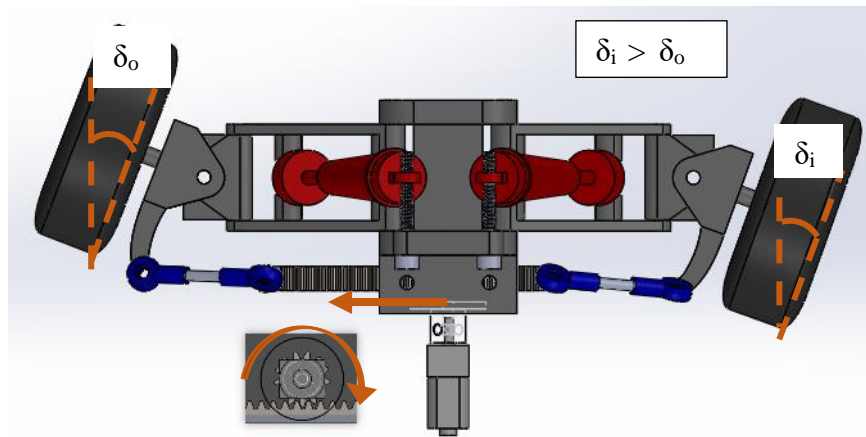


Figure 3.16: The servo motor rotates its shaft in a clockwise direction (both wheels turn right)

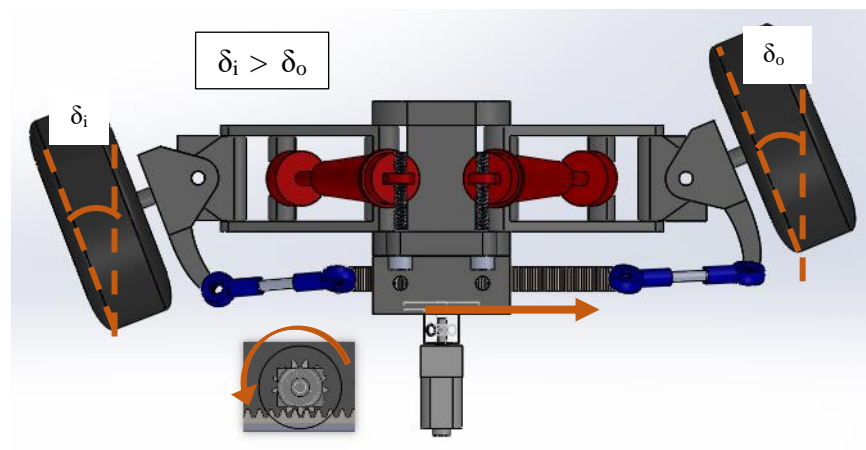


Figure 3.17: The servo motor rotates its shaft in an anti-clockwise direction (both wheels turn left)

From Figure 3.16 and Figure 3.17, the steering angle, δ of both wheel sides are different when turning right or left. The steering angle of the inner wheel, δ_i is always greater than the steering angle of the outer wheel, δ_o . This satisfies the principle of the Ackermann steering system.

3.2.6 Manipulator Design

For manipulator design, because one of the tasks of the robot is to collect the latex cups that are located at different heights, it should be designed to have a higher joint or higher DoF so as to move upward, downward, forward, and backward. Thus, 3 DoF is applied to the manipulator design. Take note that the 3 DoF stated here are just for the manipulator subfunction. 1 more DoF was on the end-effector section.

However, 3 DoF means that 3 motors are needed to operate at each joint. It is not suitable because this will increase the prototype weight and also burden the budget of the project. Thus, a manipulator design that utilises two motors to control a three DoF manipulator that was inspired by the "EEZYbotARM MK2" (Carlo, F., 2018) was implemented in our design. Figure 3.18 below shows the picture of "EEZYbotARM MK2".

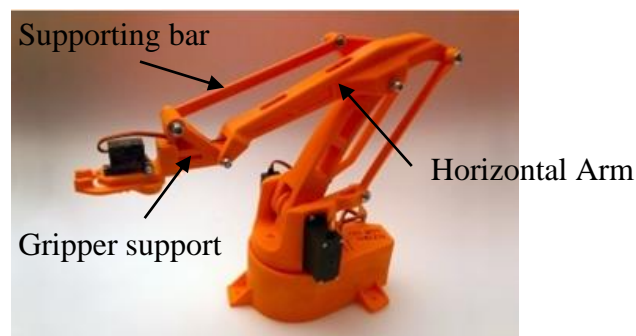


Figure 3.18: EEZYbotARM MK2 (Source: Carlo, F., 2018)

In Carlo (2018)'s design, he implemented the parallelogram mechanism that connects the horizontal arm and a supporting bar to the gripper support. The supporting bar will move together with the horizontal arm in this mechanism and stay parallel to it. This ensures that the gripper support stays parallel to the plane even though the manipulator is moving up, down, front, or rear. The gripper should stay horizontally when collecting latex cups to avoid the fallout of the liquid latex. Therefore, this design was applied and modified to the robot's needs.

The design of the manipulator was started from the base. For the base design, a circular holder was extruded out from the base (Figure 3.19). It is used to mount the main arm of the manipulator. The purpose of designing it in a circular shape is to smooth the main arm rotation without any blockage. Besides, the holder was designed to be closer to the right because on the left-hand side, some space was used to locate the horizontal arm driver level (Figure 3.20). Moreover, to reduce the centre of mass of the manipulator, two motors were also designed to be mounted on both sides of the base. The right-side motor is used to drive the main arm, while the left-side motor is used to drive the horizontal arm.

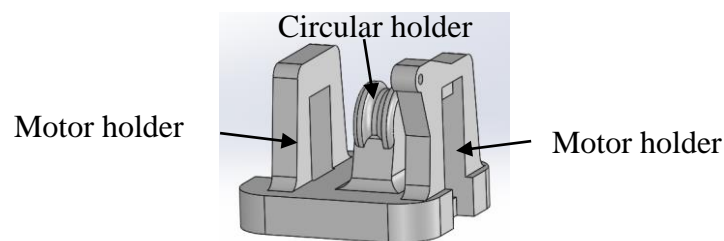


Figure 3.19: Manipulator base design in Solidworks

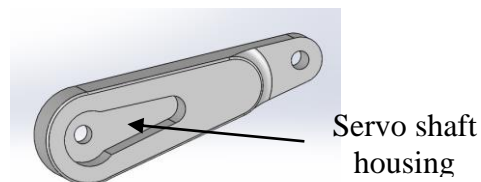


Figure 3.20: Horizontal arm driver lever

After that, the main arm was designed. The hole-to-hole length for the main arm is set at 128 mm to ensure it is long enough to extend forward for the horizontal arm and gripper to reach the targeted latex cup. Besides, the right lower part of the main arm was cut in shape to build a housing for the servo shaft that drives the main arm (refer Figure 3.21). This same goes to the horizontal arm driver lever that drive the movement of horizontal arm (refer Figure 3.20 above).

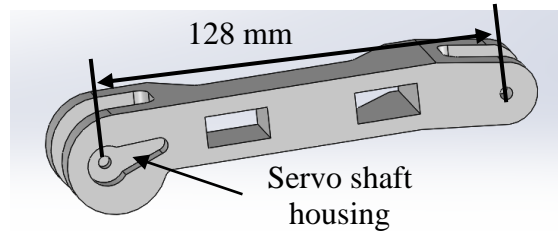


Figure 3.21: Manipulator main arm design in Solidworks

For the horizontal arm, three joint holes were designed (refer to Figure 3.22). The first joint was used to connect the gripper support, middle joint was connected to the main arm, while the last joint was designed to connect to the horizontal arm driver lever by a linkage bar that will drive the pushing and pulling of the horizontal arm.

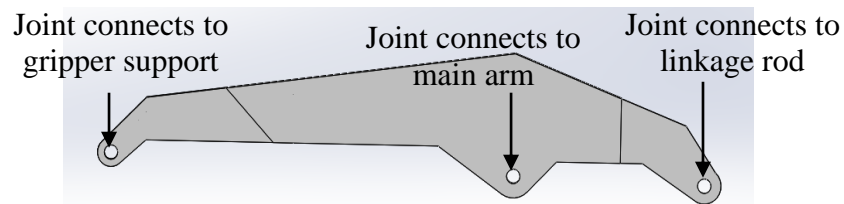


Figure 3.22: Horizontal arm design in Solidworks

Gripper support was designed as an immediate way to hold the gripper. Besides this function, the gripper support is used as a servo motor holder and the camera's chip holder (refer Figure 3.23). After that, the end of the gripper support has a cylindrical bar that is used to hold the gear and the gripper part as well. This is because the gripper part will be rotated to pour the latex into the tank.

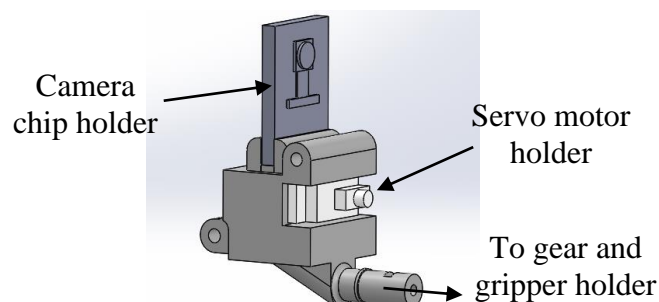


Figure 3.23: Gripper support design in Solidworks

Besides all the main parts of the manipulator, some parts act as support to the main part to perform tasks. Those parts are mostly the linkages between the main parts that fix the main parts in place. For instance, a linkage bar connects between the horizontal arm driver lever and the horizontal arm.

3.2.7 End effector Design (Gripper)

Next, a gripper end-effector was chosen instead of a suction end-effector because it requires less power and has a higher processing time as compared to suction. For the gripper design, it was designed with dimensions of 50 mm long, 20 mm wide, and 15 mm thick. Besides, the inner face of the gripper is curved in shape and has a tilting angle of 79.38 degrees. This tilting angle is to follow the angle of the latex cup design so that a better and more stable hold is ensured. Figure 3.24 shows the gripper end-effector design in Solidworks.

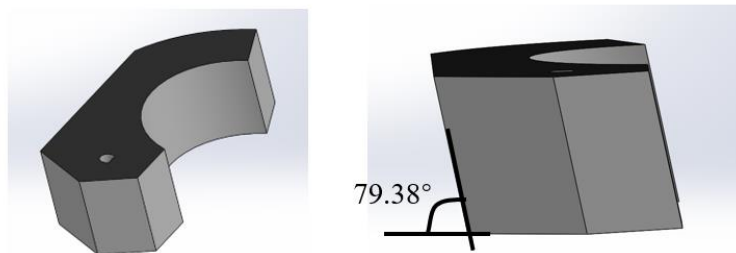


Figure 3.24: Gripper end-effector design

Besides, in order to drive the grippers' end effectors to open and close, a motor is used to turn the two gears that are mounted on each side of the gripper so that two grippers can rotate simultaneously. Thus, a motor holder was designed and placed on the top of the gripper cover. This motor holder was set to dimensions of 50 mm long and 29 mm wide, which is the same as the gripper cover. The height was 20 mm to prevent the motor from falling out. Considering that the motor will generate heat when operating, some small vents were designed for the heat to escape. Figure 3.25 shows the design of the DC motor holder and gripper holder.

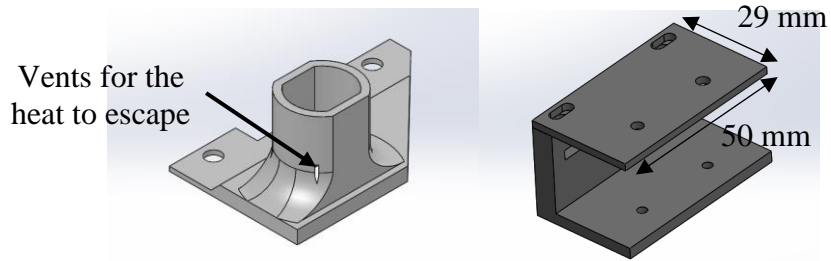


Figure 3.25: DC motor holder and Gripper holder designs

The mechanism for the pouring process was also designed with this gripper design. Two gear mechanisms, as shown in Figure 3.26, were implemented. In this mechanism, a servo motor was used to drive the small gear (10 teeth), while the big gear (15 teeth) was driven by the small gear. The gripper set was then screwed to the big gear, while the big gear was connected to the gripper support so that the gripper set was held, and rotation could be done for the pouring process.

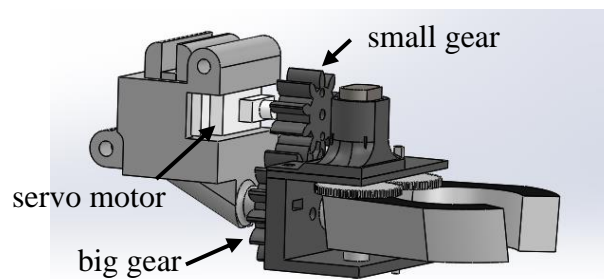


Figure 3.26: Gripper set is rotated by using the gear mechanism

3.2.8 Storage Tank Design

The storage tank was designed in a rectangular shape. Its outer dimensions are set at 90 mm long, 70 mm wide, and 27.5 mm high. The tank cannot be too high as it will block the movement of the manipulator. Also, to ease the pouring process, the funnel and pipe were designed to allow the poured latex to have a large allowance to flow into the tank easily (refer Figure 3.27). This design also prevents the latex from overflowing and spilling onto the electronic parts.

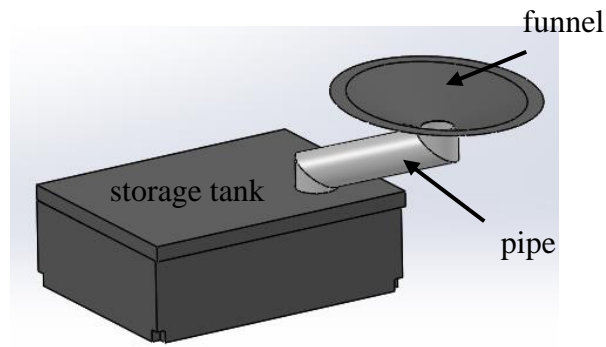


Figure 3.27: Storage tank and its supporting parts design in Solidworks

The maximum volume that can be carried by this storage tank is up to 104832 mm³ or 104.832 ml of liquid, using the formula below:

$$V_{it} = W_{it} \times L_{it} \times H_{it} \quad (3.1)$$

where

V_{it} = volume of inner tank, mm³

W_{it} = width of inner tank, mm

L_{it} = length of inner tank, mm

H_{it} = height of inner tank, mm

Moreover, the storage tank was designed to stick on the robot platform because it needed to be removed from the robot platform to get the latex inside. Thus, four male slots were designed on the platform, while four female slots were designed on the storage tank to stabilise the tank in a fixed position (refer Figure 3.28).

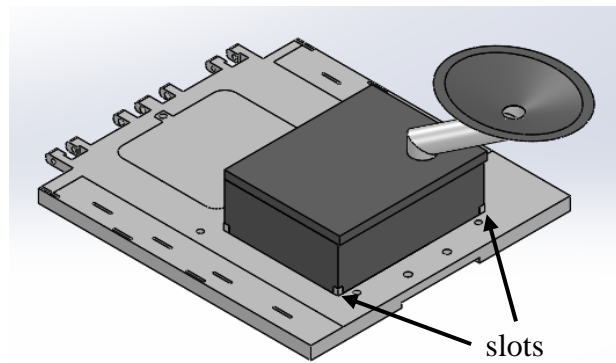


Figure 3.28: Storage tank fits into the slots on the robot platform

When all components are placed on the top of the robot platform, the stress exerted on the robot platform increases. Thus, reinforcement was designed on the other side of the platform to strengthen the platform so that it could withstand the largest force and would not deform easily. Figure 3.29 illustrates the reinforcement design under the robot platform.

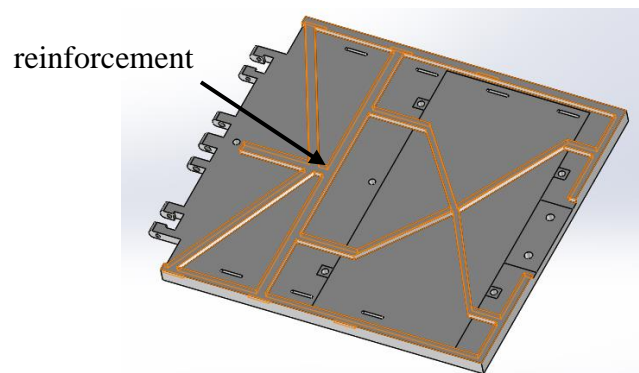


Figure 3.29: Reinforcement design under the robot platform

3.2.9 Electric components storage board

Initially, two electronic components storage boards were designed vertically (refer Figure 3.30 (a)) to utilise the vertical space as the space limitation of the robot caused those electronic components to be unable to be placed. However, vertical placement of electronic components will lead to the loosening and disconnection of wires due to gravity. Thus, the redesign was done to let the storage board be horizontal (refer Figure

3.30 (b)). But the disadvantage of the horizontal board is that it will lead to a wider design in terms of width.

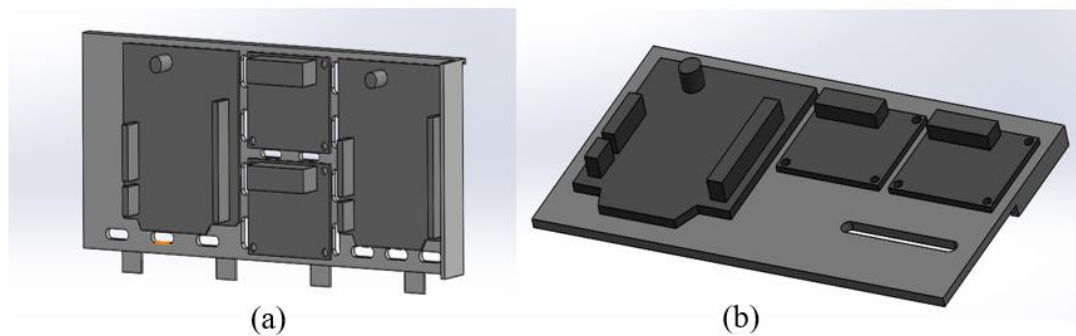


Figure 3.30: (a) Old electronic component storage board; (b) New electronic component storage board

Board covers are designed to prevent the electronic components from getting wet or latex spillage. The board cover uses the sliding feature to enclose the board as shown in Figure 3.31. Because there will be a bundle of wires attached to the electronic boards and the motors outside, the board cover was not designed to close up the full board. Space is preserved at the bottom of the cover to let inside and outside connect via wires.

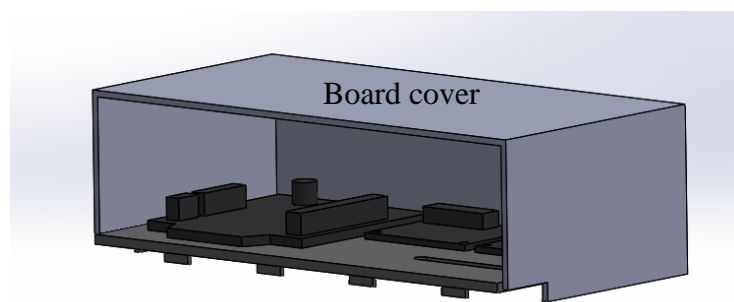


Figure 3.31: Board covers are slid to enclose the storage board

3.2.10 Base Storage Compartment

Lastly, a compartment was designed to store all the components placed below the robot platform, such as the transmission-used DC motor, steer-used DC motor, and battery holder. Two holes were designed to let the motor shafts reach outside the compartment to perform their function. After all of the components were placed inside, this compartment was bolted to the robot platform using bolts and nuts (see Figure 3.32).

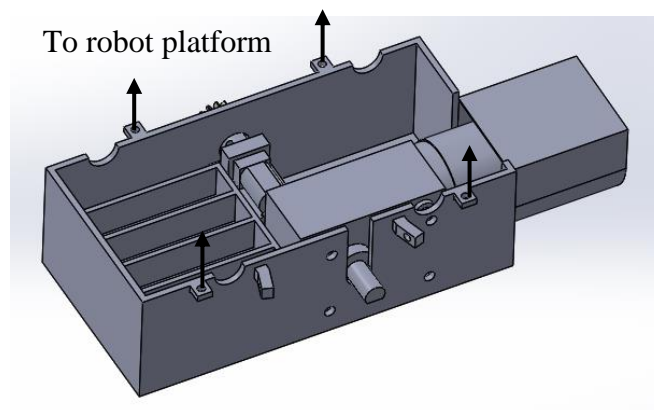


Figure 3.32: Base storage compartment filled with stored components

3.2.11 Solidworks Assembly

After all the subfunction designs were settled, they were all assembled together to become an overall prototype design. The completed prototype design was then subjected to all sorts of simulations to analyse the workability of the prototype before it was fabricated for a real-life experiment.

3.2.11.1 Mobility components

After completing the design for all the subfunctions of the mobility and steering systems, they are assembled together and stuck under the robot platform. This mobility and steering system contribute to the maximum width of 225.35 mm and the maximum

length of 301.2 mm. Figure 3.33 shows the isometric view of the complete mobility subsystem.

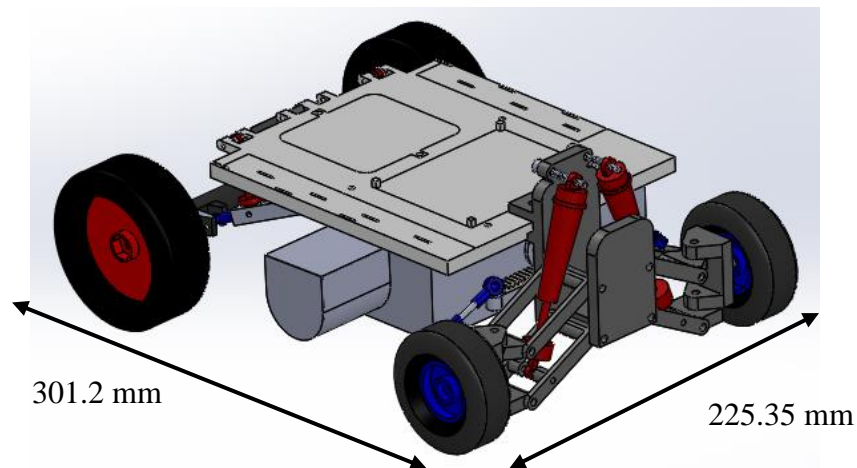


Figure 3.33: Isometric view of the mobility subsystem

3.2.11.2 Manipulation components

The M4 threaded rod, M4 washers, and M4 self-locking nuts were used to connect all of the sub-components of the manipulator and end-effector designs. Two servo motors were mounted at the base to control the movement of the main arm and the horizontal arm. Figure 3.34 shows the assembly of manipulation components in Solidworks software.

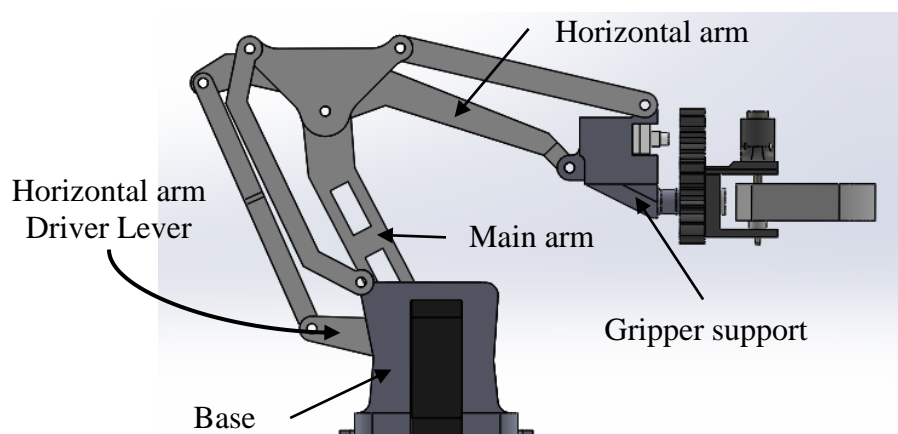


Figure 3.34: Assembly of manipulation components in Solidworks

3.2.11.3 Overall Assembly

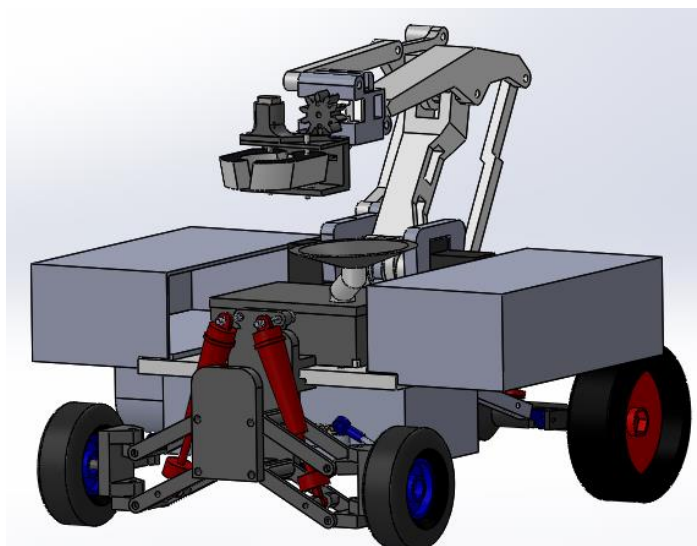


Figure 3.35: The overall prototype design of the latex cup robot collector

The overall prototype assembly is completed by the mating of the mobility component, manipulation component, and others (see Figure 3.35). The prototype designed in the Solidworks software is 301.2 mm long, 292.1 mm wide and 270.6 mm high. Besides, it weighs 2014.28 grammes.

3.3 Firmware configuration

Firmware consideration is also a crucial thing to do to ensure a functional robot. In this robot, the firmware includes DC motors and servo motors. Table 3.2 below shows the firmware selections with their specifications as well as the functions in this robot.

Table 3.2: Firmware selection and its specification

Firmware selected	Function	Specification
<p>A58SW-555 12V DC motor</p> 	<p>Drive the whole robot by converting rotational motion to linear motion through differential gear.</p>	<ul style="list-style-type: none"> • Operating voltage: 12V • Operating speed: 260 RPM • Rated current: 2A • Rated Torque: 9 kg.cm <p>(SGrobot, n.d.)</p>
<p>Arduino N20 mini-DC motor</p> 	<ol style="list-style-type: none"> 1. Use it in the rotation of the gripper to collect latex cups. 2. Use it to drive the gear and rack to steer the front wheels. 	<ul style="list-style-type: none"> • Operating voltage: 6 - 12 V • Operating speed: 60 RPM • Rated current: 0.04A • Rated Torque: 2 kg.cm <p>(LittleCraft, n.d.)</p>
<p>MG996 Servo Motor</p> 	<ol style="list-style-type: none"> 1. Drive the movement of the main arm of the robotic arm. 2. Drive the movement of the robotic arm's horizontal arm. 	<ul style="list-style-type: none"> • Operating voltage: 4.8 – 6V • Rotation angle: 0 - 180 ° • Stall torque: 12 kg.cm • Operating speed: 0.13 - 0.17 sec / 60 ° <p>(Synacorp, n.d.)</p>
<p>MG90S Micro Servo Motor</p> 	<ol style="list-style-type: none"> 1. Drive the rotation movement of the whole gripper set during the pouring process. 	<ul style="list-style-type: none"> • Operating voltage: 4.2 – 6V • Rotation angle: 0 – 180 ° • Rated torque: 1.5 kg.cm • Operating speed: 0.3 sec / 60° <p>(Synacorp, n.d.)</p>

3.3.1 Parameter calculation

After acquiring the motor's specifications, parameter calculations are performed to check the suitability of these motors for the robot.

3.3.1.1 Motor for robot transmission

According to Neal, AJ. (2010), a robot that accelerates up an incline from rest to its full speed is the condition for sizing a motor, as it will be using the maximum energy of the motor. A free-body diagram was drawn to illustrate the forces acting on the robot, as shown in Figure 3.36.

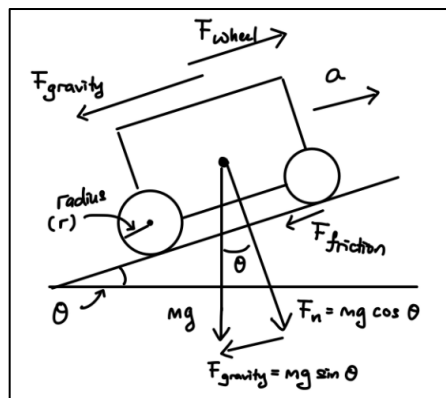


Figure 3.36: Free body diagram for robot on the inclined surface

Before starting, several parameters are defined:

- Maximum Speed of the robot, $v_{max} = 0.1$ m/s
- Initial Speed of the robot, $v_o = 0$ m/s
- Maximum incline slope to travel, $\theta_{slope} = 30$ degrees
- Time for the robot to reach maximum speed from rest, $t_a = 2$ seconds

Frictional force was assumed to be neglected to ease the calculation. Acceleration was calculated and got a value of 0.05 m/s² by using the equation:

$$a = \frac{(v_{max} - v_0)}{t_a} \quad (3.2)$$

where

a = acceleration of robot, m/s²

v_{max} = maximum speed of the robot, m/s

v_0 = initial speed (rest), m/s

t_a = Time for the robot to reach maximum speed from rest, s

With the obtained acceleration, a , the minimum output torque required to turn the wheels was calculated as 0.442 N·m by the equations:

$$\rightarrow \Sigma F = m_{robot} \cdot a \quad (3.3)$$

$$(f_{wheel} - f_{gravity}) = m_{robot} \cdot a \quad (3.4)$$

$$f_{wheel} = (m_{robot} \cdot a) + f_{gravity} \quad (3.5)$$

$$f_{wheel} = (m_{robot} \cdot a) + (m_{robot} \cdot g \cdot \sin\theta_{slope}) \quad (3.6)$$

$$f_{wheel} = \tau / r \quad (3.7)$$

$$\tau = f_{wheel} \times r \quad (3.8)$$

where

m_{robot} = mass of the robot, kg

f_{wheel} = the force pushing against the wheel, N

$f_{gravity}$ = the force pulling robot down incline due to gravity, N

θ_{slope} = Maximum slope incline to travel, degrees

τ = Torque, N·m

r = radius of the rear wheel, m

It doesn't end here. With the existing differential gear in the rear axle, gear ratio must be considered to determine the torque of the motor. Take note that the gear ratio of the differential gear is 2.5. As a result, by using the equation below, the minimum input torque required was calculated to be 0.177 Nm, which was equivalent to 1.80 kg·cm.

$$\tau_{input} = \tau_{output} / \text{Gear ratio} \quad (3.9)$$

where

τ_{input} = Torque required by the motor to drive the differential gear, N·m

τ_{output} = Output torque required by the rear wheels to drive the robot, N·m

Next, to determine how fast the motor needs to turn, the maximum speed of the robot, v_{max} , that was defined above, was used, and the value obtained was 56.17 RPM by the equations:

$$RPM_{output} = \frac{v_{max}}{2\pi \times r} \quad (3.10)$$

$$RPM_{input} = \text{gear ratio} \times RPM_{output} \quad (3.11)$$

where

v_{max} = maximum speed of the robot, m/min

r = radius of rear wheel, m

RPM_{input} = Rotational speed required by the motor to drive the differential gear,
rev/min

RPM_{output} = Output rotational speed required by the rear wheels to drive the robot,
rev/min

As a result, the selection of the A58SW-555 12V DC motor in **Table 3.2** above is suitable for the robot transmission as the minimum torque required (1.80 kg·cm) and the speed required (56.17 RPM) for the motor is within the specification of the selected motor.

3.3.1.2 Motor for robotic arm

Robotic arm is another part that requires a motor to drive the movement. In this section, the main arm of the robotic arm was analysed to determine the torque. This is because the torque experienced by the main arm must not exceed the motor's stall torque, or else the motor will not hold the arm and the arm will fall. Figure 3.37 below illustrates the forces exerted on the main arm that result in the torque. F_A represents the weight of the main arm while F_B represents the other parts that are connected after the main arm (e.g., arm 2, support, connector, and gripper, which can refer to Figure 3.40 below).

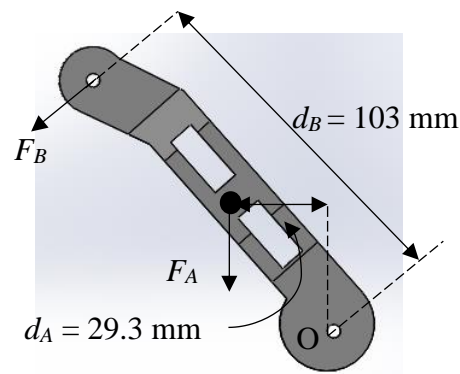


Figure 3.37: Forces acting perpendicular to point O on the main arm

By using the equation below, the torque exerted on point O, τ_O is 0.1729 N·m, which is equivalent to 1.763 kg·cm.

$$+ccw \tau_O = \sum F_n \times d_n \quad (3.12)$$

where

F_n = Force exerted perpendicular to the point O, where n = A and B, N

d_n = Distance between F_n and point O, where n = A and B, mm

As a result, the use of the MG996 servo motor on the main arm is suitable because the stall torque of this servo motor is 12 kg·cm while τ_O is just 1.763 kg·cm which is safe to operate without falling. Take note that the same type of servo motor is also used to control the horizontal arm. However, no calculations were performed

on it because it will also be functional since the motor can function on main arm that experience more torque.

3.3.1.3 Motor for gripper rotation (Pouring)

The mass moment of inertia was included in the calculation to calculate the torque required by the gripper to rotate. This is because the pouring process needs angular movement, and the mass moment of inertia is the ability to accelerate angularly.

First, the gripper set was separated into three different parts, namely parts A, B, and C (Figure 3.38). Next, the mass moment of inertia of these three parts was determined by using Solidworks software. Before that, the angular velocity, ω for the pouring process was set as 8 rev/min for 2 seconds. The angular velocity was then converted to rad/sec to ease the calculation process by using the formula:

$$\omega \text{ (rad / s)} = \omega \text{ (rpm)} \times \frac{2\pi}{60} \quad (3.13)$$

where

ω = angular velocity, rad/s

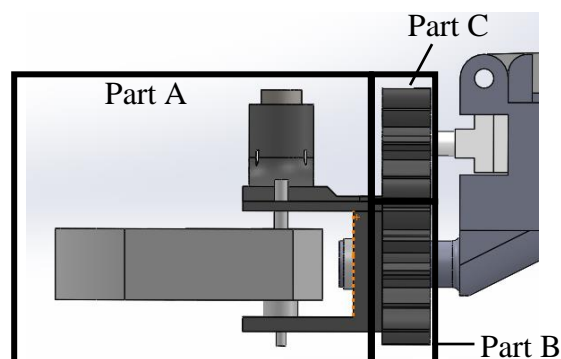


Figure 3.38: 3 separated parts of gripper set

The mass moments of inertia for parts A and B are summed up to determine the total inertia needed to rotate these two parts. This is because these two parts are mounted together and rotate together. After that, the torque needed to rotate parts A and B was calculated by using the equation:

$$\tau_{\text{part 1 \& 2}} = I_{\text{part 1 \& 2}}\alpha = I_{\text{part 1 \& 2}}\left(\frac{\omega}{t}\right) \quad (3.14)$$

where

$\tau_{\text{part 1 \& 2}}$ = torque required for part 1 and part 2, N·m

$I_{\text{part 1 and 2}}$ = mass moment of inertia of part 1 and 2, kg·m²

α = angular acceleration, rad/s²

t = time, s

After determining the torque required for parts A and B, it is used to calculate the torque required for the motor to rotate part C. Gear ratio is also involved here and it can be determined by using the formula:

$$\text{Gear ratio, } GR = \frac{\text{Gear Teeth}_{\text{driven}}}{\text{Gear Teeth}_{\text{driving}}} \quad (3.15)$$

Besides, the torque for part C is calculated by using the formula:

$$\tau_{\text{part 3}} = I_{\text{part 3}}\left(\frac{\omega(GR)}{t}\right) + \frac{(\tau_{\text{part 1 and 2}})}{GR} \quad (3.16)$$

As a result, the torque required for the motor to rotate the full gripper for pouring is 5.94×10^{-6} N·m, which is equivalent to 6.06×10^{-5} kg·cm. The selected motor for this was the MG90S, with a rated torque of 1.5 kg·cm. Thus, it is more than enough to rotate the gripper.

3.4 Static Analysis

Static analysis was conducted in order to ensure the designed prototype could be fabricated and assembled properly without any breakdown. It was used to calculate the effects of constant loads on the mechanical structure by using a computational tool called Finite Element Analysis (FEA). Luckily, Solidworks software has provided this FEA tool to perform static analysis. Two components (robot platform and robotic arm) underwent this FEA analysis because these two components experience the largest load and have the highest chance of breaking.

Before the analysis, the weight of all the parts was determined so that they could be used as the loads in the analysis. The weight of the designed parts from Solidworks was estimated through the software with the settings of PLA material. While other components, like motors, were determined by weight balance. The quantities we obtain will be in mass units, which will then be converted to weight (in Newton) by using the formula below:

$$W_c = m_c \times g \quad (3.17)$$

where

W_c = weight of component, N

m_c = mass of component, kg

g = gravity, m/s^2

3.4.1 Robot Platform

The robot platform is the part that has the most loads acting on it. At the top of the robot platform, the loads are composed of the electronic components, storage tank, and robotic arm. While at the bottom of the platform, the load exerted is the base storage compartment, which consists of motors and batteries inside. Split lines of various shapes were drawn to represent different components (see Figure 3.39).

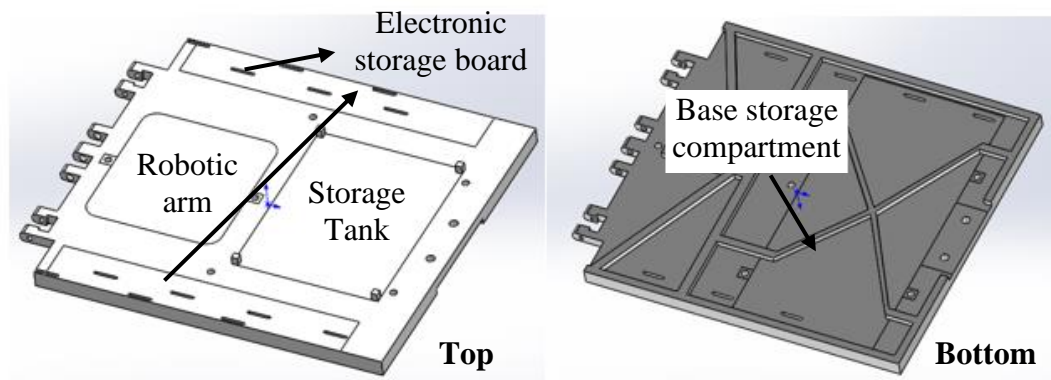


Figure 3.39: Split lines for different loads exerted on robot platform (top & bottom)

After that, forces were calculated using equation (3.17) above and then added within the split lines for each of the components. Table 3.3 below shows the weight and forces for each component acting towards the robot platform. Take note that all the components mentioned were built up from several sub-components, and the values shown below are the sum of all those sub-components.

Table 3.3: Loads acting on the robot platform

Components	Weight (g)		Force (N)
Storage tank filled with water	117.90 (storage tank) + 102.10 (water)	210	2.06
Electronic storage (Left)	110 (printed board) + 80 (chips)	190	1.86
Electronic storage (Right)	110 (printed board) + 70 (chips)	180	1.77
Base storage compartment	86 (compartment) + 140 (battery) + 428 (12V DC motor) + 10 (5V DC motor)	664	6.51

For the robotic arm, the whole assembly has a weight of 0.35 kg. However, it cannot be directly applied to the platform as it will undergo retraction and extension to perform collection tasks, whereas other components are fixed in their position. When the robotic arm is extended, it will exert compression and tension effects on the platform. This is because the centre of mass of the extended arm is not within the

base's designated area, shown in Figure 3.40 as the blue colour line. So, calculation is needed to find out the specific forces. Figure 3.40 shows the simplified robotic arm's free body diagram under extended condition (the critical condition). Take note that the centre of mass of each part was determined by using Solidworks. Then the distances determined were the distances between the centre of mass and Point A (refer Figure 3.40). The weight of the parts is also shown in Table 3.4 below:

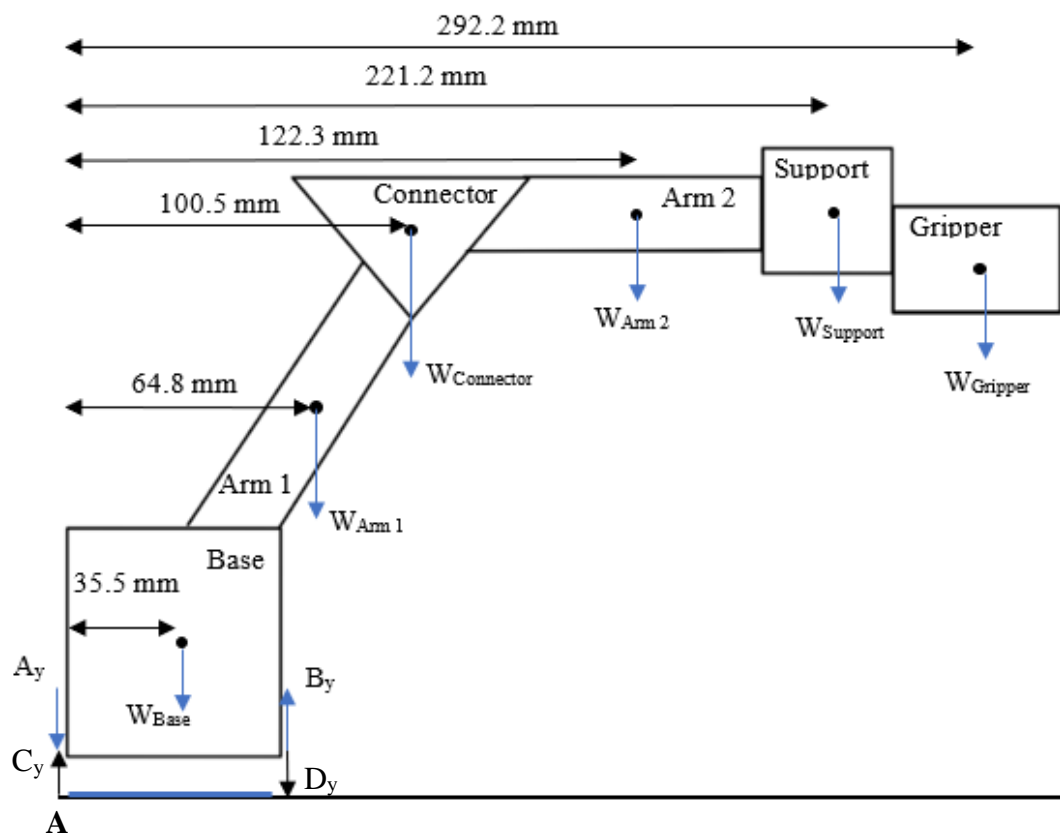


Figure 3.40: Free body diagram for the robotic arm

Table 3.4: Weight of each part of robotic arm

Components	Weight (g)		Force (N)
Base	42.0 (printed part) + 57.0 (Servo motor) + 57.0 (servo motor)	156.0	1.53
Arm 1	25.5 (printed part)	25.5	0.25
Connector	9.0 (printed part)	9.0	0.088
Arm 2	27.5 (printed part)	27.5	0.27

Support	28.74 (printed part) + 12.0 (SG90 servo motor)	40.74	0.40
Gripper (With latex cup)	25.0 (printed parts) + 16.0 (grippers) + 35.51 (latex cup filled with water) + 10 (N20 motor)	86.51	0.85

After obtaining all the information and parameters needed, the equilibrium equation was used to calculate the forces acting on the platform by the robotic arm:

$$+ \uparrow \sum F_y = 0 \quad (3.18)$$

$$- A_y - W_{base} + B_y - W_{Arm1} - W_{Connector} - W_{Arm2} - W_{support} - W_{Gripper} = 0 \quad (3.19)$$

$$+ cw \sum M_A = 0 \quad (3.20)$$

$$W_{Base}(35.5) - B_y(71.0) + W_{Arm1}(64.8) + W_{Connector}(100.5) + W_{Arm2}(122.3) + W_{Support}(221.2) + W_{Gripper}(292.2) = 0 \quad (3.21)$$

$$A_y = -C_y \quad (3.22)$$

$$B_y = -D_y \quad (3.23)$$

where

F_y = forces acting at the Y direction, N

U_y = forces acting on point U in the Y direction, where U = A, B, C, and D, N

M_A = moment at point A, N·mm

After solving the equations, the forces obtained are 2.94 N and 6.33 N for C_y (tension) and D_y (compression), respectively. These two values are then applied to two square faces that represent the fastening points for the robotic arm and robot platform (see Figure 3.41).

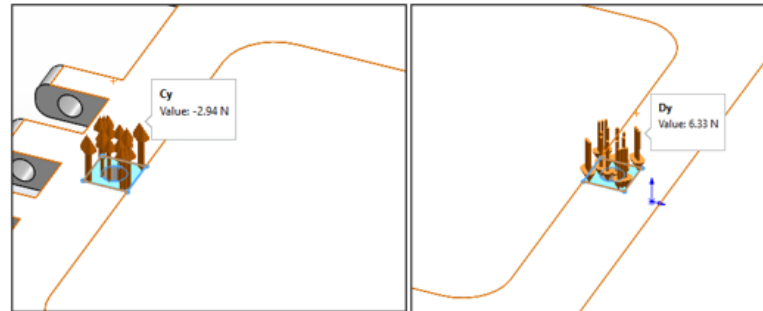


Figure 3.41: Forces exerted by the robotic arm on the robot platform

Moreover, in order to avoid certain areas of the robot platform from deforming, a fixture feature was also applied within the spline line area. For example, the back of the robot platform does not wish to be deformed as it is screwed with the shock damper of the rear wheel part. Thus, the fixture hinge was applied to it, as shown in Figure 3.42.

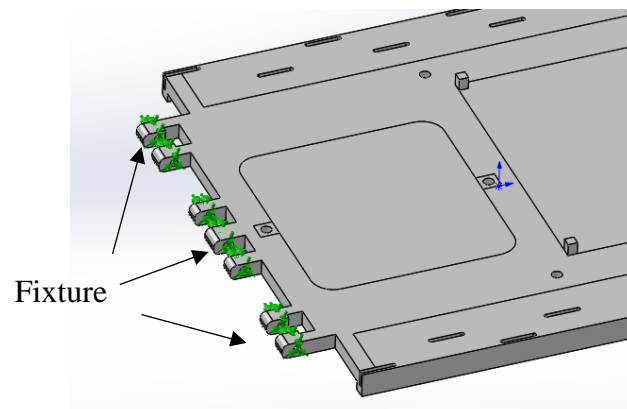


Figure 3.42: Fixture applied on the bank of the robot platform

3.4.2 Robotic Arm

For static analysis of robotic arms, the critical condition (which is during the arm's extension to collect latex cup) is used to determine the maximum stress, displacement, and strain. Unlike the robot platform, only one load (which is a latex cup filled with water) was applied to the gripper, and the value was 0.348 N. Next, a fixture was

applied to the base of the robotic arm. Moreover, due to the many joints designed on the arm, the pin connection feature was applied to every joint to prevent the joint from deforming during the simulation. Figure 3.43 shows the settings of the robotic arm in Solidworks.

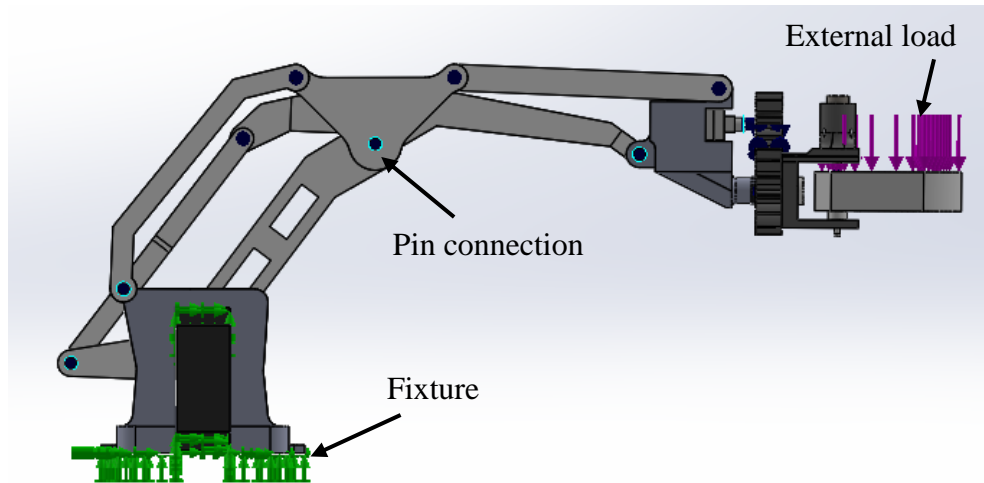


Figure 3.43: Static analysis settings for robotic arm in Solidworks

3.5 Centre of mass: Toppling analysis

Toppling analysis is one of the most important things to determine the stability of a mobile robot. This is because we can obtain the maximum incline angle that can be overcome by the robot without overturning. Thus, toppling analysis was performed to get a brief idea of how high an incline the designed robot can handle.

3.5.1 Centre of mass identification

The centre of mass of the robot was first determined because the centre of mass should be held within the robot's footprint and once it falls outside it, a topple will occur. Thus, the formulas below are used to calculate the centre of mass for each direction (X, Y, and Z):

$$x_{cg} = \frac{\sum_1^n m_n g x_n}{\sum_1^n m_n g} \quad (3.24)$$

$$y_{cg} = \frac{\sum_1^n m_n g y_n}{\sum_1^n m_n g} \quad (3.25)$$

$$z_{cg} = \frac{\sum_1^n m_n g z_n}{\sum_1^n m_n g} \quad (3.26)$$

where

$n = 1, 2, 3 \dots, n$

x_{cg} = centre of gravity in X direction relative to a point, mm

y_{cg} = centre of gravity in Y direction relative to a point, mm

z_{cg} = centre of gravity in Z direction relative to a point, mm

n = number of parts

m_n = mass of parts, g

x_n = centre of gravity of that component n in X direction relative to a point, mm

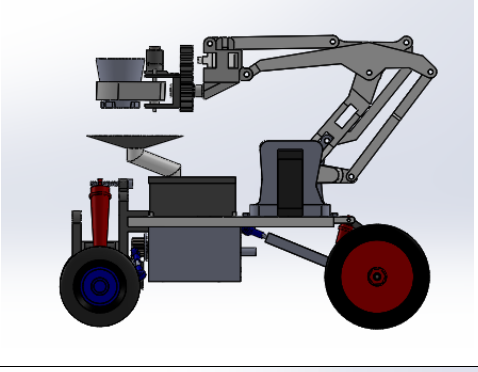
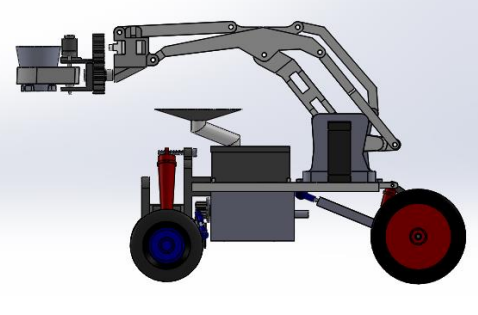
y_n = centre of gravity of that component n in Y direction relative to a point, mm

z_n = centre of gravity of that component n in Z direction relative to a point, mm

However, this will be a complicated calculating process as this robot involves a lot of parts and components. Luckily, Solidworks software provides an easier way to solve this problem. The centre of mass can be easily generated by the software itself by choosing the "Centre of Mass" feature.

The different positions of the robotic arm and the mass of the robot will change the position of the centre of mass of the robot due to the shifting of weight. Thus, four scenarios that include all the processes of the robot are created. These four scenarios are shown in Table 3.5 below. Take note that only heavy parts and components are included so as to simplify the analysis and also because the light mass has an insignificant effect on the centre of mass.

Table 3.5: Four scenarios of centre of mass identification

Scenario	Arm	Tank	Picture
1	Retracted	Empty	
2	Retracted	Full	
3	Extended	Empty	
4	Extended	Full	

3.5.2 Topple Angle

After determining the centre of mass of the robot, the topple angle was determined by using the results obtained from the centre of mass. The topple angle was calculated for four sides, which are the front, rear, left, and right of the robot for each scenario. This is to indicate whether the robot can operate in the rubber plantations, which have unstructured terrain. Figure 3.44 shows the free body diagram of the left topple and back topple. Based on Figure 3.44, formulas to calculate the topple angle are:

$$\theta_{topple} = 90^\circ - \alpha \quad (3.27)$$

$$\alpha = \tan^{-1}\left(\frac{Y}{X}\right) \quad (3.28)$$

where

θ_{topple} = topple angle, °

Y = vertical distance of centre of mass from the floor, mm

X = horizontal distance of centre of mass from the robot side, mm

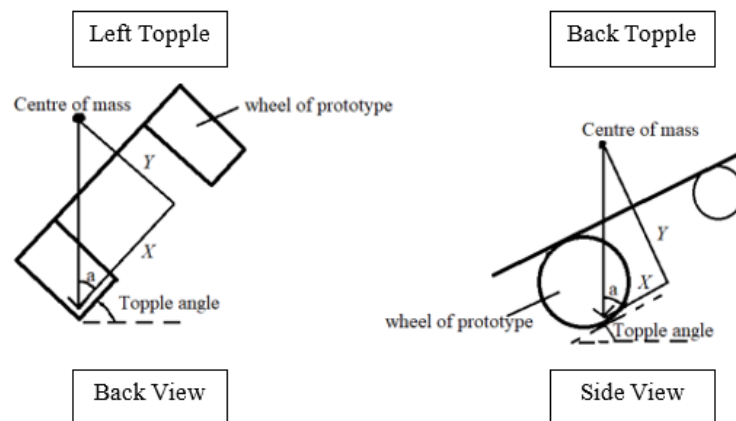


Figure 3.44: Free body diagram of left topple and back topple

3.6 Motion Study

Besides the FEA simulation, motion study also been done by using the Solidworks software. The purpose of this motion study is to determine the dynamic performance of the mobility subsystem for the robot design when encountering unstructured terrain.

First, to illustrate the scenario of the real-world terrain, a simple uneven track with barriers was built (refer Figure 3.45). For the barriers, they were designed with a 15 mm height and an incline of 45° and 50° , respectively. They are built at different locations to test for scenarios that can be confronted by the robot. Those scenarios include: i) left wheels encounter the barrier; and ii) right wheels encounter the barrier.

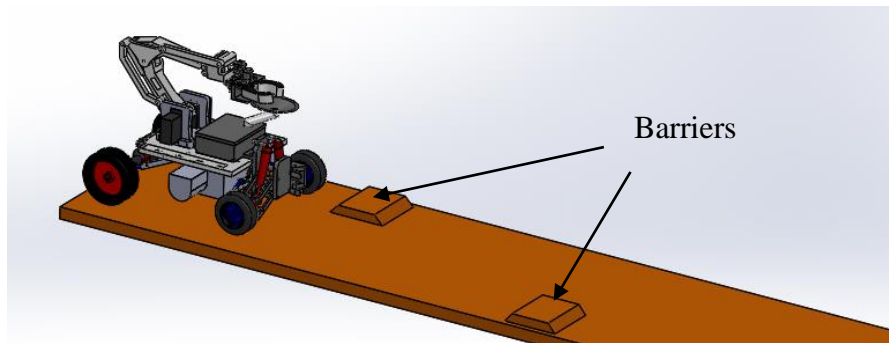


Figure 3.45: Uneven track built for Motion Study in Solidworks

After that, the designed robot and track were added to a new assemble file to start the setting of the motion study. The first thing was to add the gravitational force to the system to simulate the real-life environment. In this case, a default of 9806.65 mm/s^2 is exerted on the robot itself on the Z-axis, which is pointing downward to the track.

3.6.1 Motor Feature

After that, the motor feature is set to the rear axle. Suppose the motor feature has to be applied on the motor shaft, but in order to reduce the constraint calculated, it was applied on the rear axle and the speed set was 56 RPM, which was already considered the gear ratio calculated in Section 3.3.1.1. Figure 3.46 below shows the motor feature settings in Solidworks software.

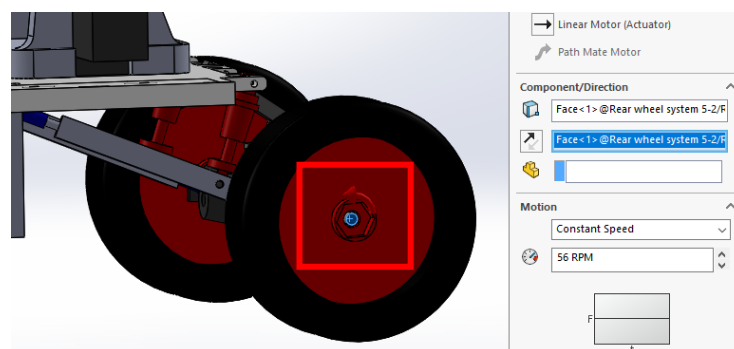


Figure 3.46: Motor feature setting for motion study

3.6.2 Spring Feature

Next, the spring feature is set to the suspension system's spring. Because of the limited information about the spring and shock damper provided by the seller, the spring constant of the springs has been obtained by using the compression test (refer Figure 3.47).

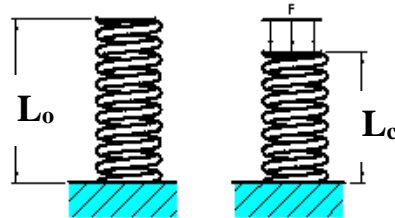


Figure 3.47: Compression test conducted on the spring and shock damper

In the compression test, the spring and shock damper were compressed to determine the compression length of the spring, L_c . The force exerted will be represented by the 500 g load and the compressed length was measured by using the ruler three times to get the average. The experiment was repeated by increasing the 500g load to 2000g. After that, the spring constant was determined by calculating the slope from the graph of the weight of loads, F_s vs spring stretch, x , using the equations:

$$x = L_0 - L_c \quad (3.29)$$

$$k = \text{Slope} = \Delta F_s / \Delta x \quad (3.30)$$

where

L_0 = Initial spring length, mm

L_c = Compressed spring length, mm

k = spring constant, N/mm

F_s = weight of loads, N

x = spring stretch or compression, mm

Following the experiment, the spring constants for the front-wheel and rear-wheel systems were determined. And the results are 0.6258 N/mm and 0.1264 N/mm, respectively. Figure 3.48 below illustrates how the spring constant for the spring of the front wheel is obtained.

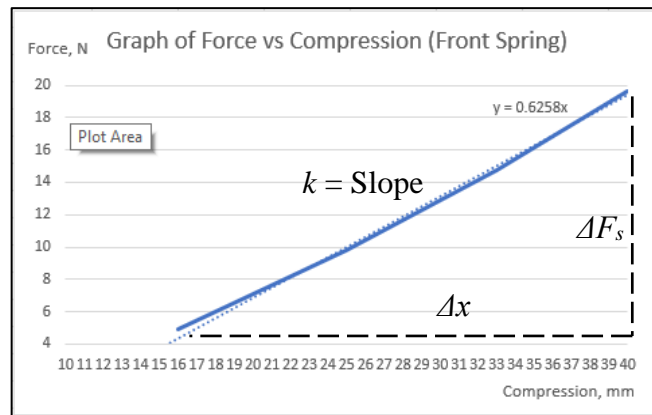


Figure 3.48: Graph of spring constant calculation for front spring

After that, these values were input into the spring constant of the spring feature. Other parameters such as the spring width, number of cells and wire diameter were measured and keyed into the setting for a more precise simulation to be done on the robot.

3.6.3 Contact Feature

The last setting is the contact between the robot wheels and the track surface. In this setting, the friction coefficient will be used to get a better simulation result. Static and kinetic friction coefficients are both included in this setting. However, it is hard and there is no optimal method to determine the friction coefficients. Thus, internet sources have become the method to get friction coefficients. Choosing the surfaces on wheels on concrete, the static and kinetic friction coefficients obtained are 1 and 0.8, respectively (Townsend, 2002), then key in the contact feature.

After getting all the settings done, the motion study was started. Then the result was observed to evaluate the availability of the designed robot to encounter the barrier built on the track.

3.7 Fabrication of Prototype and Experiment Set up

All the designed parts were fabricated by using two 3D printers in the IE lab of UTAR, which are the Creality Ender 3 and the Flashforge Dreamer 3D printer. The difference between these two 3D printers is that the Flashforge Dreamer was used to print the parts that will carry and store the water, such as latex cups, latex tank, funnel, and pipe. This is because the layers printed by this printer are thicker, avoiding the gap between layers, which makes the water not transferrable between boundaries. The material used for the printing was PLA plastic because it has a lower printing temperature and is biodegradable as compared to ABS plastic (Giang, n.d.).

After converting all the 3D drawings to stereolithography (STL) files, the files are opened in the slicing software to make settings related to infill factors (pattern and density), layer thickness, number of shells, and support and raft enablers. Other parameters like infill angle and printing speed are set according to the situation too. When the setting is completed, they will be converted again to g-code files for the 3D printer to print the parts.

For parts printed by Dreamer Ender 3, the infill pattern used is the cubic pattern with the infill density of 25%–40% according to the strength required for the part. While for Flashforge Dreamer, the infill pattern used is hexagon, and with the infill density of 30%, as there is no cubic pattern in the setting of this software. Other than that, other parameters are set with the same values for both software. For example, layer thickness is set to 0.2 mm, the number of shells is 4, and the printing speed is set to 60 m/s.

3.7.1 Experiment setup

3.7.1.1 Topple test setup

This test was conducted to verify the calculation of the topple angle for the prototype in Chapter 3.4.2. An adjustable laptop stand is used to act as the incline surface for the prototype to lie on (Figure 3.49). This laptop stand has eight different angles, which are 10°, 20°, 27°, 31°, 25°, 28°, 42° and 45°. The prototype was placed on the laptop stand at the first angle. After that, the incline angle was increased until the prototype toppled. In Chapter 3.4, four scenarios were included, but, in this test, only two scenarios where the latex tank was empty were involved to prevent the water overflow and damage the electronic components.



Figure 3.49: Laptop stand for the topple angle test

3.7.1.2 Prototype test run

For the prototype test run, the prototype first underwent functional tests that required it to perform the tasks assigned to it. Two 1.5-litre water bottles were used as "rubber trees" with 30 cm between each rubber tree (see Figure 3.50) to simulate a real rubber plantation. This is because, according to Qi et al. (2015), rubber trees normally have a spacing of 2.5–3 m within a row. So, with a scale of 10, each bottle was separated by

30 cm. Moreover, to test the flexibility of the robotic arm, latex cups were placed at three different heights on three water bottles (refer Figure 3.51). Lastly, two printed barriers were placed on the robot's travel path for it to get through to observe whether it could pass them. Besides, its platform movement was observed too and compared with the motion study conducted in Chapter 3.6. Figure 3.52 shows the barriers setup in the left and right wheel directions.

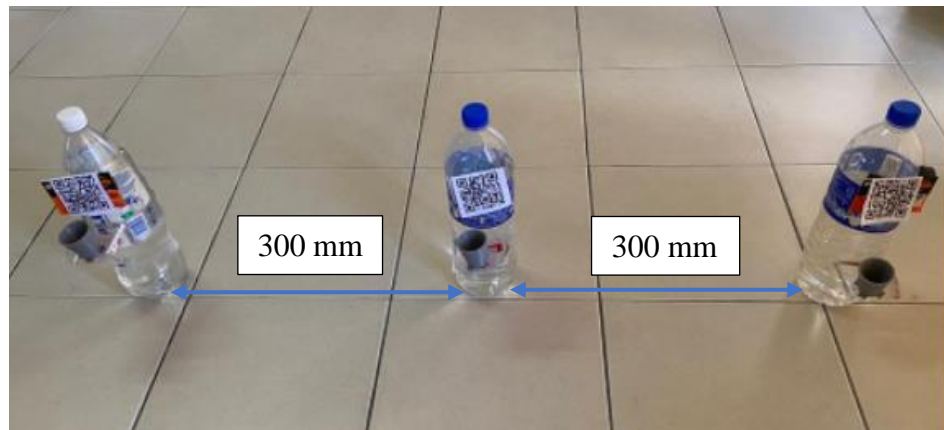


Figure 3.50: Experiment floor setup

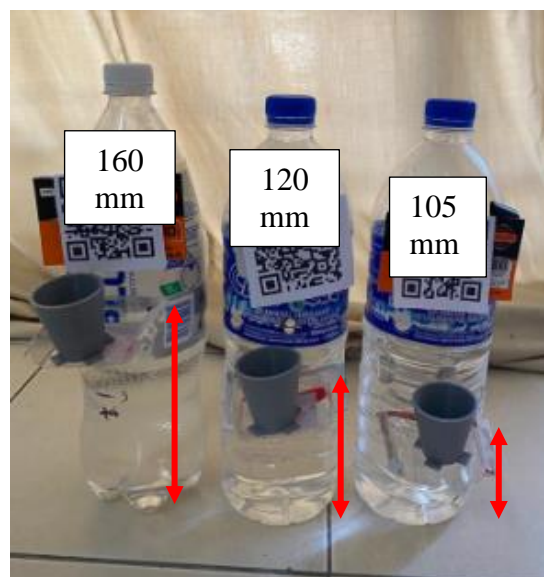


Figure 3.51: Latex cups at 3 different heights on “rubber tree”

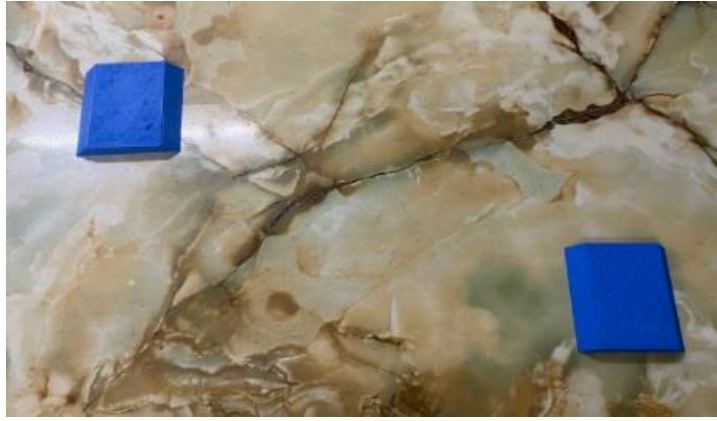


Figure 3.52: Experiment floor setup for mobility test

3.8 Project Planning and Milestone

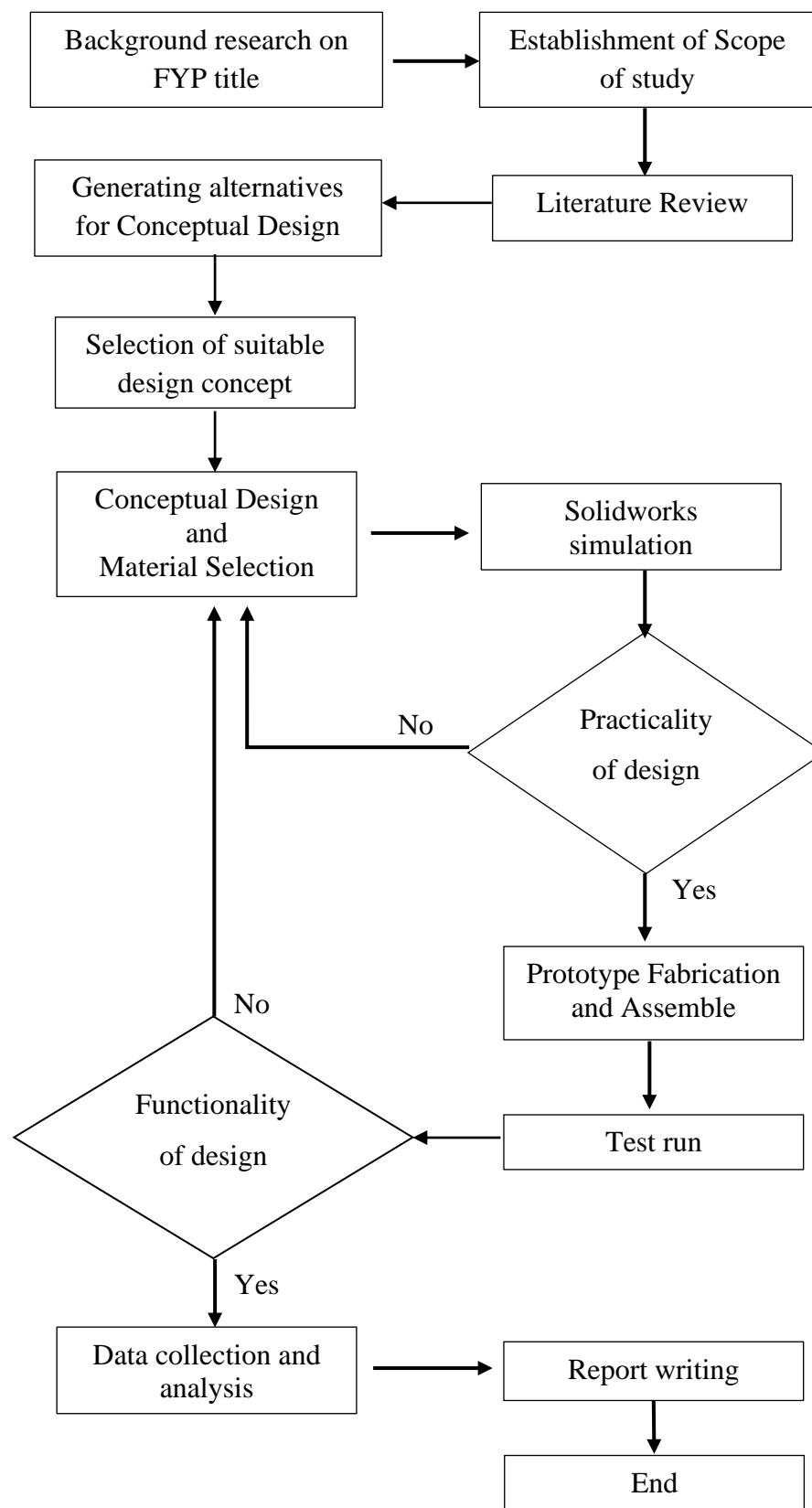


Figure 3.53: The project's overall flowchart

Figure 3.53 above shows the overall flow of this project. It will be divided into two phases to complete the whole project, which are FYP 1 and FYP 2. The duration of this project is one year.

In FYP 1, after the title of the final year project was decided, background research was conducted to get a better understanding of the title. From that, the scope of this study was then established to set a goal and limitations for this project. After that, literature reviews of previous researchers' articles were conducted to grasp the ideas from them to improve and modify the design of this project. Alternatives of the component design concepts were generated and discussed to choose a suitable design for the final conceptual design. After deciding on the final design for each component, the design process was started by using Solidworks software. At the same time, suitable materials and components that should be bought outside were researched and selected to get the dimensions so that the design could be drawn fitly. Besides, simulation set up is also done after the completion of prototype design.

For FYP 2, the simulation was run to validate the design and determine whether or not it worked. If an error occurs, amendment of the CAD design would be done before the prototype fabrication. After that, prototype fabrication and assembly were carried out. The trial run was then performed on the fully assembled prototype to ensure that the overall robot can operate and function properly. The prototype robot is tested in different types of scenarios to perform its task. Calibration and design amendments would be carried out when the prototype is not able to fulfil the scope of this project. After the final version of the prototype is established, data collection for the experiments, such as the operation time per cycle, is recorded and analysed accordingly. After all, report writing is continued to complete the project.

Two Gantt charts, Figure 3.54 and Figure 3.55, as shown below, represent FYP 1 and FYP 2, respectively. These two charts are used in this project to determine the project planning schedule and keep track of the project's progress.

No.	Project Activities	W1	W2	W3	W4	W5	W6	W7	W8	W9	W10	W11	W12	W13	W14
M1	Background research on FYP title	Planned	Planned												
		Actual	Actual												
M2	Establishment of Scope of study			Planned	Planned										
			Actual												
M3	Literature Review and Generating alternative for Conceptual Design					Planned	Planned	Planned							
				Actual	Actual	Actual	Actual								
M4	Conceptual Design, Material Selection and Simulation Build Up					Planned									
					Actual										
M5	Report Writing								Planned	Planned	Planned	Planned	Planned		
								Actual	Actual	Actual	Actual	Actual			

Figure 3.54: FYP 1 Gantt Chart



No.	Project Activities	W1	W2	W3	W4	W5	W6	W7	W8	W9	W10	W11	W12	W13	W14
M1	Simulation Run	Planned													
		Actual													
M2	Prototype Fabrication and Assemble	Planned													
		Actual													
M3	Test run, Calibration and Amendment	Planned													
		Actual													
M4	Data collection and Analysis	Planned													
		Actual													
M5	Report Writing	Planned													
		Actual													
M6	Presentation	Planned													
		Actual													

Figure 3.55: FYP 2 Gantt Chart



CHAPTER 4

RESULTS AND DISCUSSIONS

4.1 Latex Cup Collector Robot prototype

The prototype was done by assembling all the printed parts, necessary firmware, and completing the wire connections of the control system. Take note that the electronics parts were settled by another partner from the Electronics Engineering Department. Figure 4.1 shows the latest version of the prototype. From its appearance, it looks almost the same as what is designed in Figure 3.35. For better illustration, Figure 4.2 shows more views (front, rear, left, and right) of this prototype. Besides, this prototype has dimensions of about 285 mm in length, 290 mm in width, and 270 mm in height. It is also 2266 grammes in weight, which is 251.72 grammes different from the weight obtained using Solidworks software. This is because miscellaneous weights such as fasteners and wires have added weight to the robot prototype. Thus, this might affect the experiment results being different from the simulation results.

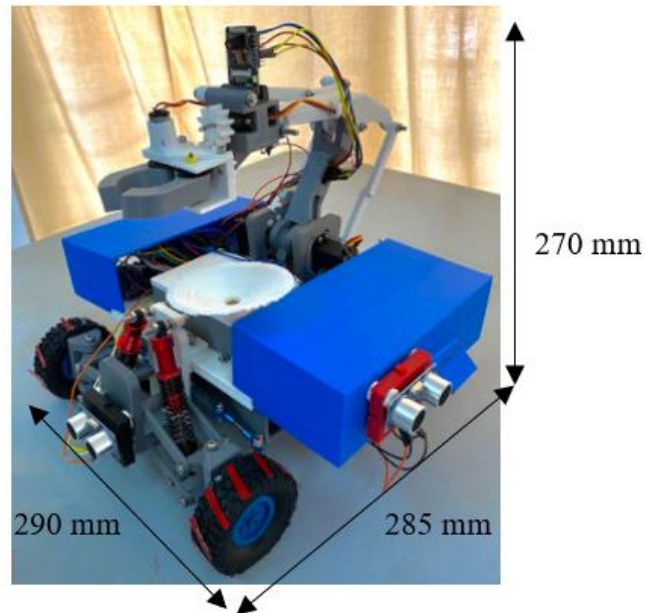


Figure 4.1: Prototype of the Latex Cup Collector Robot (Isometric view)

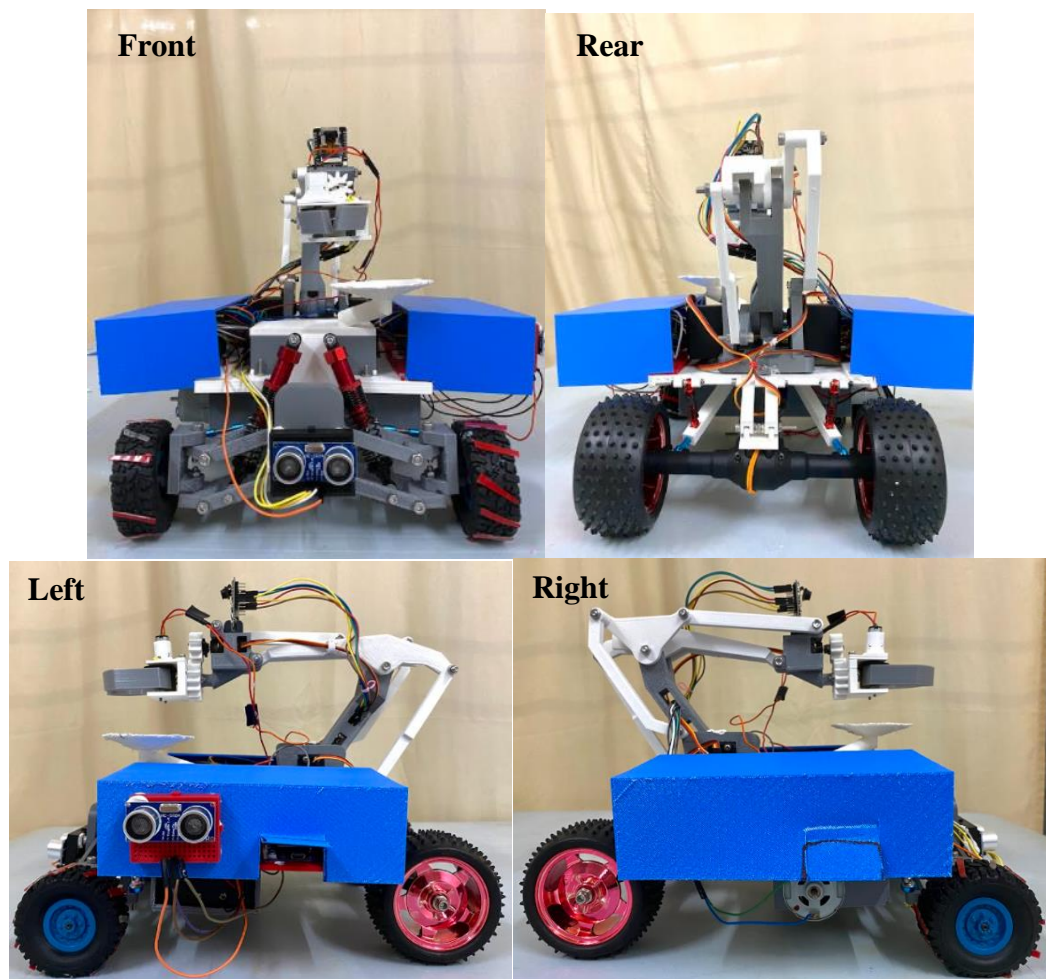


Figure 4.2: Four different views of the prototype

4.2 Finite Element Analysis (Static Test)

In FEA simulation, three types of plots were obtained, which are the stress plot, displacement plot, and strain plot. A stress plot is used to show the forces that are exerted on the body and that tend to deform the body. Besides, a displacement plot is used to know how much deformation will occur from the original position. While a strain plot is the change in length of the body that is deformed.

4.2.1 Robot Platform

This section shows and discusses the FEA results of the robot platform during its robotic arm being extended. It is noted that this scenario is where the robot platform experiences the maximum forces exerted on it.

From Figure 4.3, the stress obtained is between $5.213 \times 10^2 \text{ N/m}^2$ (minimum) and $2.589 \times 10^6 \text{ N/m}^2$ (maximum). The maximum stress is exerted on the front fastening point of the robot platform with the robotic arm. This result makes sense because the weight of the whole robotic arm is supported by that point when the robotic arm extends to collect latex cups. However, it is still feasible to be used and will not break as the maximum stress is not beyond the yield strength of PLA plastics (the printing material of the robot platform). Besides, the second largest stress (green zone) is exerted at the centre front of the robot platform. This is because there are forces from the upper and bottom sides of the platform. There is a latex storage tank placed on top of it, while a base storage compartment is placed at the bottom that exerts downwards tension forces on the robot platform.

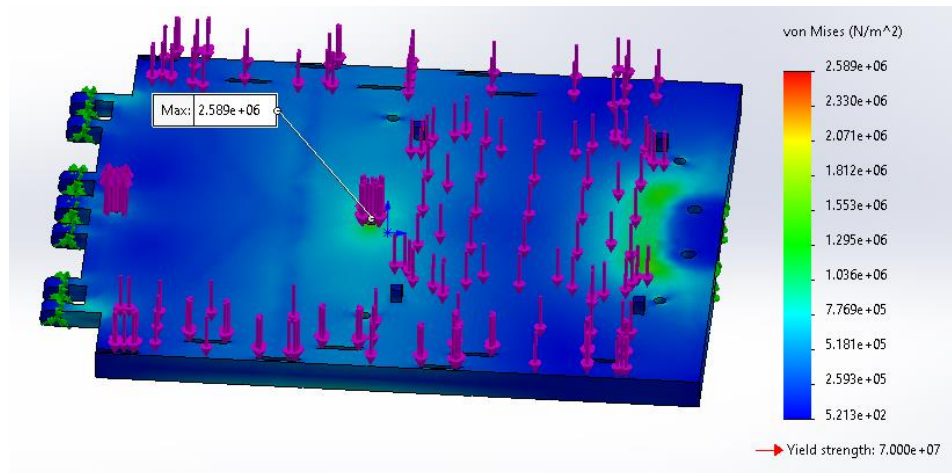


Figure 4.3: Stress plot for the robot platform

The maximum displacement obtained for the robot platform is 1.494×10^{-1} mm. From Figure 4.4, it can be observed that the robot platform deforms largely towards the centre, and the red zone that represents the largest deformation is on two sides of the robot platform's centre. This is because all the designed components are located at the centre of the robot platform, making them heavier and causing them to deform more in that area. The result of this plot immediately shows the effect in the real case of the robot platform. From Figure 4.5, it shows a slight bend at the centre of the prototype's platform after a few days of assembly. This also verifies that the working concept of FEA simulation discussed in Chapter 3.4.1 is clear and correct.

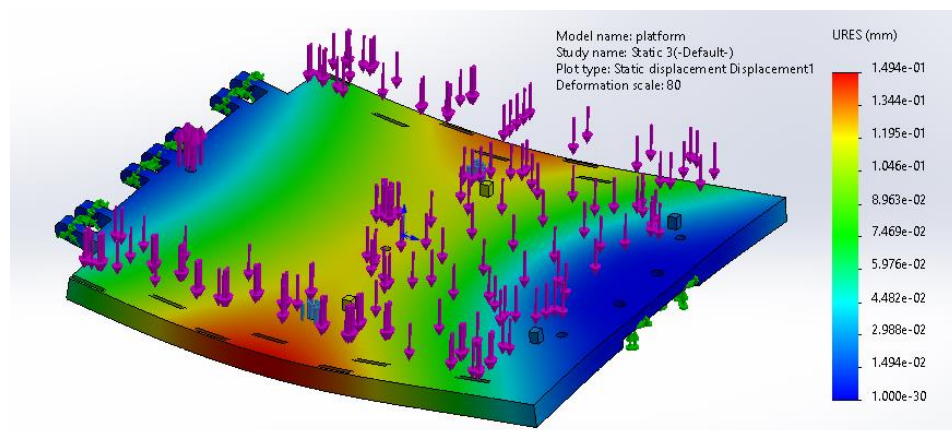


Figure 4.4: Displacement plot for the robot platform

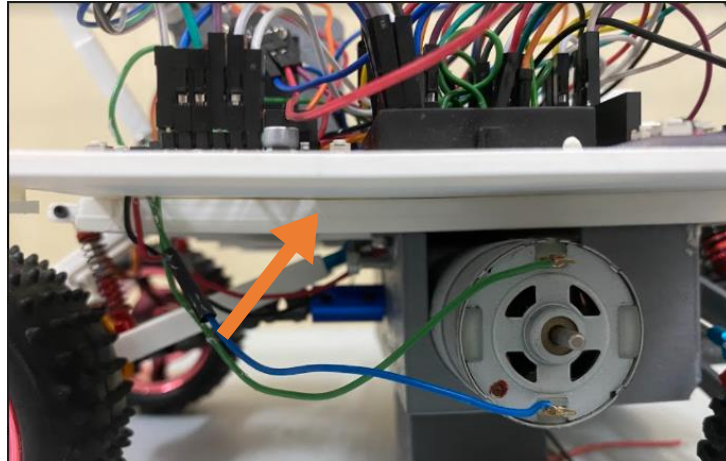


Figure 4.5: Deformation happens on the printed robot platform

For the strain result, Figure 4.6 shows that the maximum strain is located at the same place as the stress plot, which is the front fastening point of the robot platform with the robotic arm. It has the largest change in length as compared to the original length, with a ratio value of 3.551×10^{-4} mm/mm. When converted to a percentage, it is around 0.03%, which did not result in any robot platform failures.

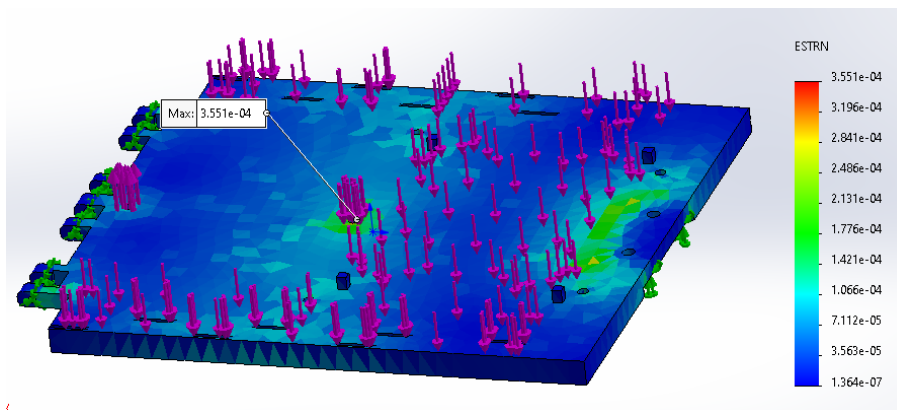


Figure 4.6: Strain plot for the robot platform

4.2.2 Robotic Arm

This section shows and discusses the FEA results of the robotic arm being extended to collect a latex cup filled with water. It is noted that in this scenario, the robotic arm encounters the maximum forces exerted on it.

From Figure 4.7, we observed that the stress exerted on the robotic arm lies between $2.894 \times 10^{-6} \text{ N/m}^2$ and $8.676 \times 10^5 \text{ N/m}^2$. The stress exerted on the robotic arm is lower than that on the robot platform. This is due to fewer external loads being carried by the robotic arm as compared to the robot platform. The inner part of the gripper is where the robotic arm experiences the most stress. Figure 4.8 shows the section view of the inner section of the gripper to better identify the specific location. It is observed that the exact maximum stress is exerted on the motor shaft that rotates the open and close of the gripper. Moreover, from both Figure 4.7 and Figure 4.8, it can be observed that for every part, the area surrounding the joints (or fastening points) has higher stress as compared to the rest. This is because stress will concentrate around the hole and may lead to premature structure failure when load is exerted via fasteners (Abdullah, Abdullah and Samad, 2019).

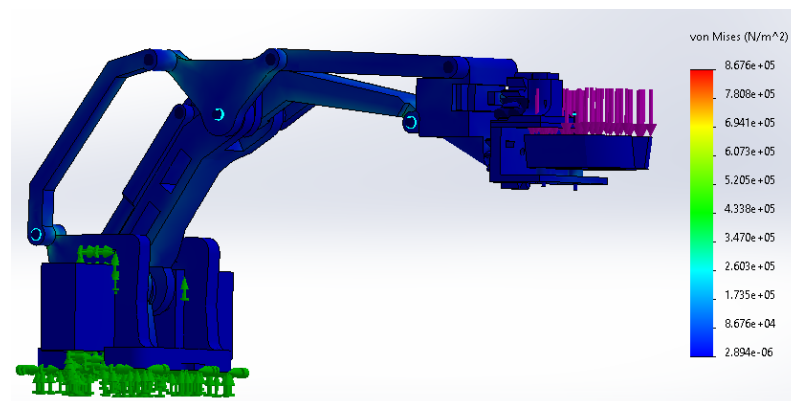


Figure 4.7: Stress plot for the extended robotic arm

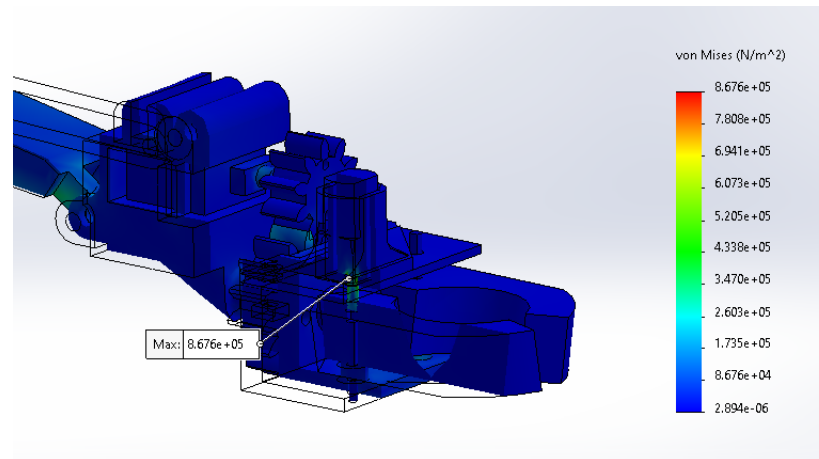


Figure 4.8: Section view of the gripper part (stress plot)

From Figure 4.9, it is observed that the robotic arm has a maximum displacement of 1.868×10^{-1} mm at the end of the left gripper. The reason why the left gripper deforms more than the right gripper is that the right gripper is supported by the motor shaft, which is made of metal, while the left gripper is supported by a PLA printed shaft. This is also why the motor shaft will exert the maximum stress as compared to others, because it will not deform easily. Besides, because of the large weight of the gripper support, it is also displaced largely from its original position, as shown in Figure 4.9.

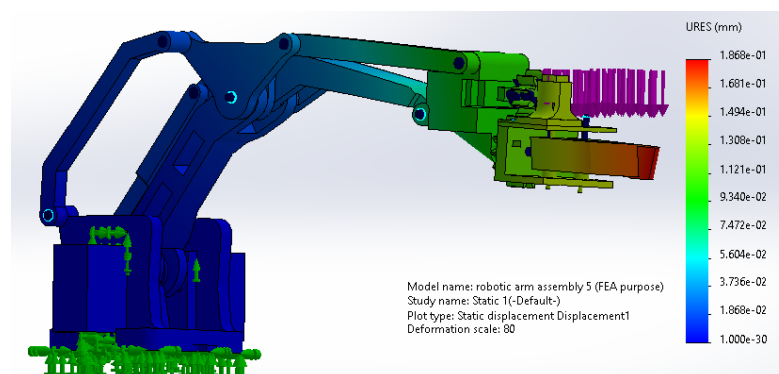


Figure 4.9: Displacement plot for the extended robotic arm

Moreover, for the strain results from Figure 4.10, the largest change in length towards the original length is located at the bottom joint of the main arm, with the highest value of 1.683×10^{-4} mm/mm. This is mainly because, at that point, it needs to

support and withstand all the following parts. Torsion force exists at the cross section of the joint and results in the highest value of strain.

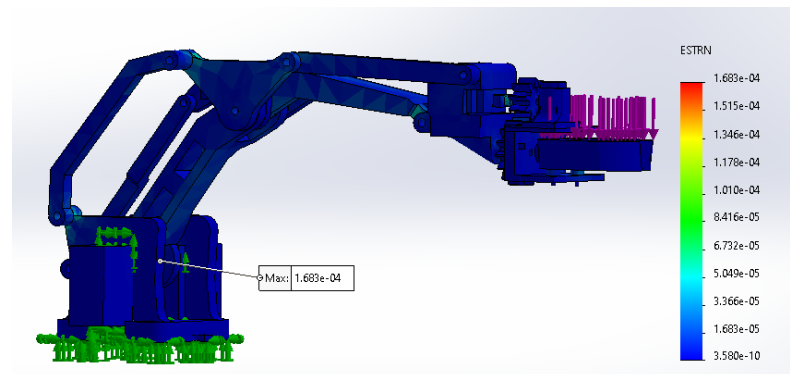


Figure 4.10: Strain plot for the extended robotic arm

4.3 Centre of Mass: Toppling Analysis

This section shows the results for Chapter 3.5, which covers the centre of mass of the designed robot under four different scenarios and also the topple angle calculation of the robot under these scenarios. With the prototype ready, the results of the topple angle experiment (discussed in Chapter 3.7.1.1) are determined in this section too.

4.3.1 Centre of mass

As mentioned in Chapter 3, four different scenarios are used to calculate the centre of mass. Figure 4.11 shows how the measurements of x, y, and z-direction of the centre of mass were made and Table 4.1 shows the results obtained from the Solidworks software.

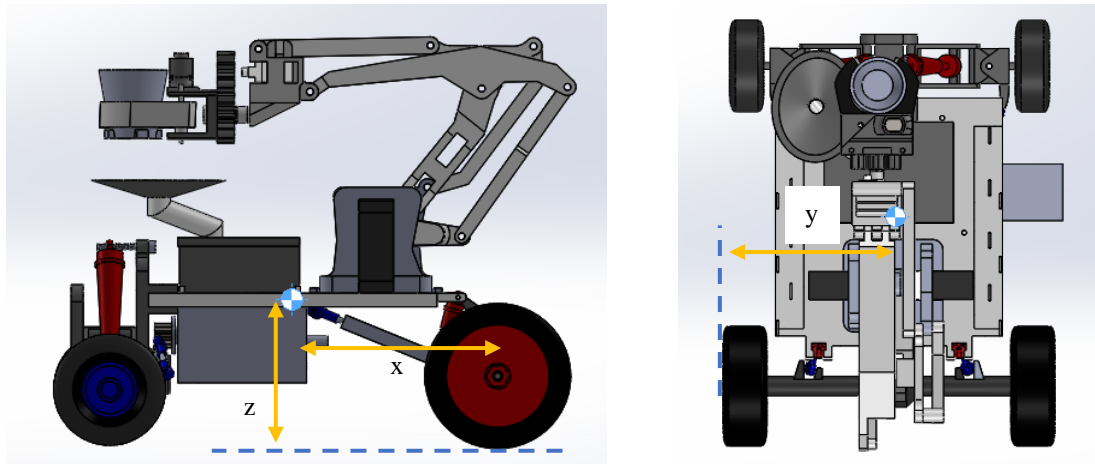


Figure 4.11: Measurement of centre of mass from each direction

Table 4.1: Centre of mass of designed robot for 4 different scenarios

Scenario	Arm	Tank	x (mm)	y (mm)	z (mm)
1	Retracted	Empty tank	119.18	122.21	86.92
2		Full tank	119.83	122.02	87.35
3	Extended	Empty tank	132.08	122.21	86.35
4		Full tank	132.51	122.02	86.79

From Table 4.1, it is observed that the centre of mass in the y and z directions of the robot has just slight changes among the 4 different scenarios. However, the centre of mass changes largely in the x direction. When the robotic arm extends to collect the latex cup, the centre of mass moves forward to 132.08 mm for an empty tank and 132.51 mm for a full tank. This will lead to a smaller front topple angle when the robotic arm extends too. But luckily, the centre of mass of the designed robot for all four scenarios is located within the four wheels, ensuring the prototype does not overturn when travelling and operating on a flat surface.

4.3.2 Topple Angle

With the results of the centre of mass in Table 4.1 above, the topple angles for all four scenarios were calculated using formulas (3.27) and (3.28), and the results are shown in Table 4.2 below.

Table 4.2: Calculated topple angles for four different scenarios

Scenarios		Topple angle (°)			
		Front	Rear	Left	Right
Retracted	Empty tank	50.88	53.90	54.58	52.13
	Full tank	50.57	53.91	54.40	52.04
Extended	Empty tank	47.42	56.82	54.76	52.32
	Full tank	47.15	56.78	54.58	52.22

From Table 4.2, it is observed that the left and right topple angles are almost the same for the four different scenarios. This is because of the insignificant changes in y and z directions for the centre of mass. While the front and rear topple angles have significant changes when the robotic arm changes. Front topple angles decrease by about 3°, while rear topple angles increase by about 3° when the robotic arm extends. This is due to the change in the centre of mass in the x direction.

Next, the experimental topple angles were determined too, after the prototype was built, to verify the calculated topple angles. However, only two scenarios were used for this verification, which were the prototype with an empty tank and robotic arm retracting and the prototype with an empty tank and robotic arm extending. This is to prevent water spillage and any inconvenient causes. Table 4.3 below shows the results for the experimental topple angles. Calculated topple angles are also included in this table to calculate the percentage error between the two results obtained. The percentage error is calculated by using the formula:

$$\text{Percentage error (\%)} = \frac{|\text{calculated angle} - \text{experimental angle}|}{\text{experimental angle}} \times 100\% \quad (4.1)$$

Table 4.3: Calculated and Experimental topple angles and their % error

Scenario	Topple Angle (°)				
		Front	Rear	Left	Right
Retracted & Empty tank	Calculation	50.88°	53.90°	54.58°	52.13°
	Experiment	45°	45°	50°	50°
	% Error	13.07%	19.77%	9.16%	4.26%
Extended & Empty tank	Calculation	47.42°	56.82°	54.76°	52.32°
	Experiment	38°	48°	48°	49°
	% Error	24.79%	18.38%	4.67%	6.78%

From Table 4.3, it is observed that all the experimental topple angles are smaller than the calculated topple angles. This is mainly because, in the experiment, all the components are included, while only significant components are included in the calculation. This affects the position of the centre of mass on the prototype and then leads to the smaller topple angle. In terms of percentage error, it can be observed that left and right topple angles have a percentage error below 10%, but front and rear topple angles have a percentage error above 10% and below 25%. This may be due to the suspension system of the prototype. As the prototype tilts toward the wheels, the spring will slightly compress, causing the prototype's centre of mass to shift. So, the topple angles will decrease as well for the front and rear directions.

However, from Table 4.3, it is observed that the minimum angle of incline that the prototype can travel across without toppling is 39° if the robot has enough power to travel. And this angle is more than enough for the prototype to travel through the rubber plantation.

4.4 Prototype test run

This section shows the results of two tests discussed in Chapter 3.7.1.2. The first one is the functional test that requires the prototype to operate on one cycle of the latex collection process. The second test is the manipulator test, which is used to test the flexibility of the robotic arm to collect latex cups from different heights. Take note that all tests are conducted indoors to avoid prototype spoilage due to unforeseen circumstances and to make the testing process easier.

4.4.1 Functional test

As mentioned in Chapter 3, water bottles are used to represent rubber trees. Before starting, the water bottle was placed 600 mm on the left-hand side of the prototype. The reason why 600 mm was chosen is that this prototype needed space to turn to the target. After all the setup was completed, the test run started. The working process can be separated into three parts: two for the mobility subsystem (turns into tree and reverses back to track), while the other one is for the manipulator subsystem (latex cup collecting operation). Figure 4.12 shows the video snapshots of the working process for the prototype to collect the latex cups for one cycle. While Table 4.4 lists down the step-by-step actions and the cycle time recorded for every action. A total of 26 commands (actions) are used for the prototype to complete one cycle, and the total cycle time is approximately 107 seconds, which is 1 minute 47 seconds per working cycle. The cycle is then repeated when it reaches the next water bottle.

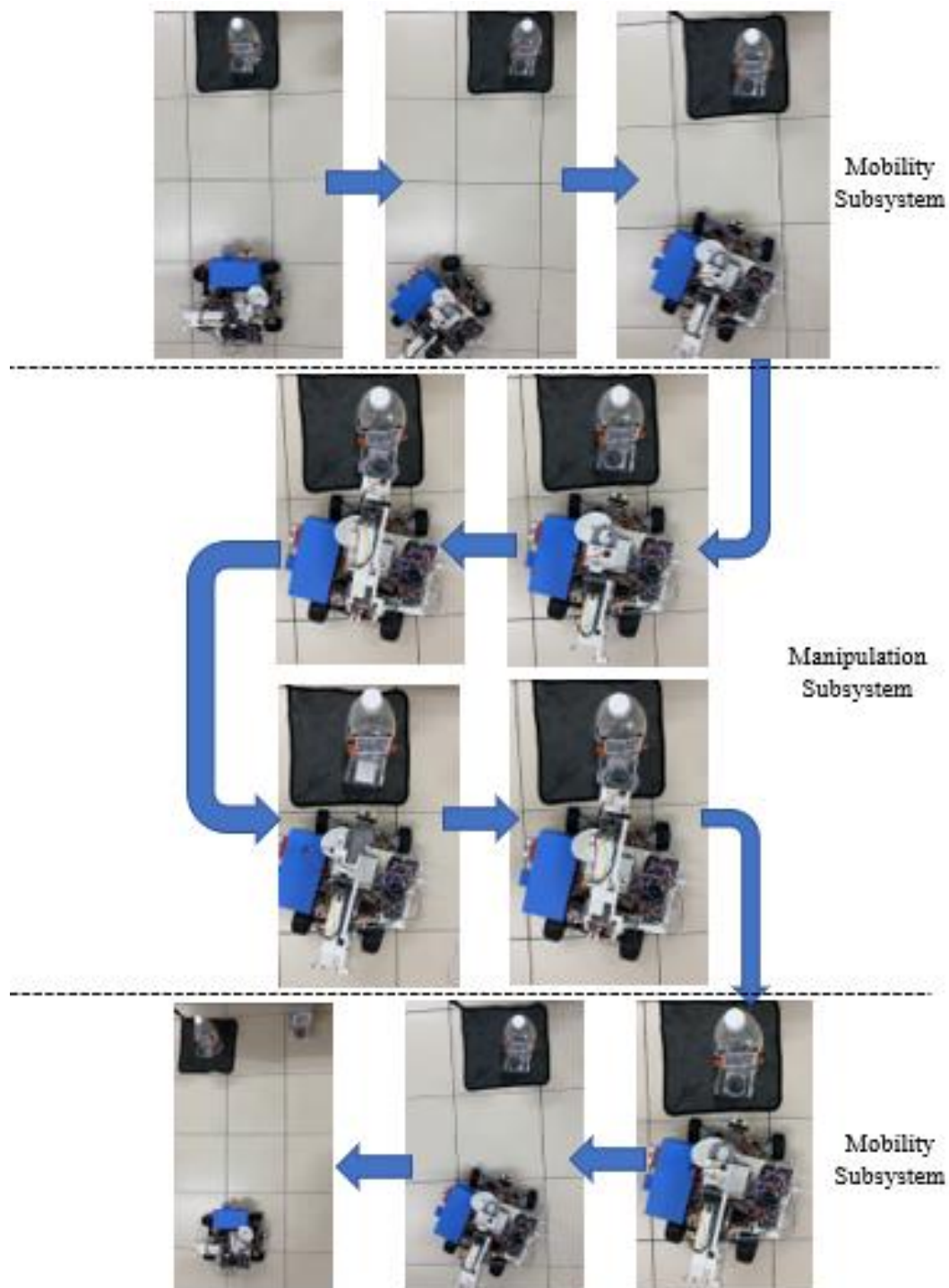


Figure 4.12: Working process for the prototype to collect the latex cups for a cycle

Table 4.4: Step-by-step action and its cycle time

Stage	Working Subsystem	Action	Time (second)
1	Mobility	Prototype stop (after bottle sensing)	3
2		Steering turn right	3
3		Prototype reserves	12
4		Steering return centre	3
5		Steering turn left	2
6		Prototype travel to bottle	11
7		Prototype stop	1
8	Manipulation	ESP32 scanning QR code	4
9		Gripper opens	3
10		Arm extends (to reach target)	3
11		Stop	1
12		Gripper closes	3
13		Stop	2
14		Arm retracts	3
15		Gripper rotates anti-clockwise	6
16		Stop	1.5
17		Gripper rotates clockwise	2
18		Arm extends	6.5
19		Gripper opens	4
20		Arm Retracts	3.5
21	Gripper closes	2	
22	Mobility	Prototype reserves	13
23		Steering returns centre	1
24		Steering turn right	1
25		Prototype travels to reposition (back to straight line)	11
26		Steering returns centre	1
Total cycle time			106.5

4.4.2 Manipulator Test

In this test, three different heights of latex cups are placed on three water bottles. The heights are 160 mm, 120 mm, and 105 mm, respectively, from the ground. Three QR codes that store the height values of the latex cups are pasted on top of the water bottles to indicate three different heights for the robotic arm to grab the latex cups, then the codes are scanned by the ESP32 camera on top of the robotic arm. After that, the robotic arm will perform its task based on three different cases. Figure 4.13, Figure 4.14, and Figure 4.15 show the video snapshot of the working process of the robotic arm to collect latex cups at a height of 160 mm, 120 mm, and 105 mm, respectively. By observing the video snapshots, the robotic arm was able to perform perfectly to collect the cups at different heights.

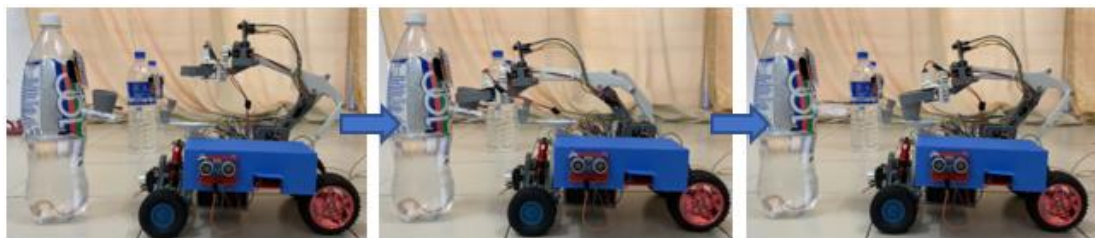


Figure 4.13: Robotic arm collects latex cup at 160 mm height



Figure 4.14: Robotic arm collects latex cup at 120 mm height



Figure 4.15: Robotic arm collects latex cup at 105 mm height

4.5 Mobility Test

For this mobility test, the Solidworks motion study and a real-world experiment were carried out to validate the results obtained from each other. The results obtained for both tests are the pitch, yaw, and roll of the prototype. Pitch is the rotation about the y-axis of the body, yaw is the rotation about the z-axis of the body, and roll is the rotation about the x-axis of the body as respect to the centre of mass. Figure 4.16 illustrates the rotation of pitch, yaw, and roll on the prototype design, and this concept will be used in the following subsection.

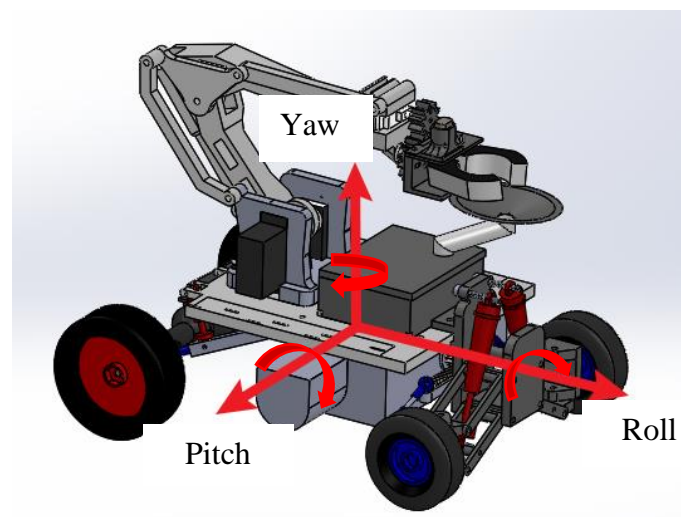


Figure 4.16: Pitch, yaw, and roll illustration

4.5.1 Motion Study

After the simulation of motion study is done, the pitch, yaw, and roll angles are obtained for the results. Figure 4.17 below shows the combined graph of these three angles of the designed robot after encountering two barriers. Take note that the clockwise rotation along each axis is positive while the anti-clockwise rotation is negative for these three rotations.

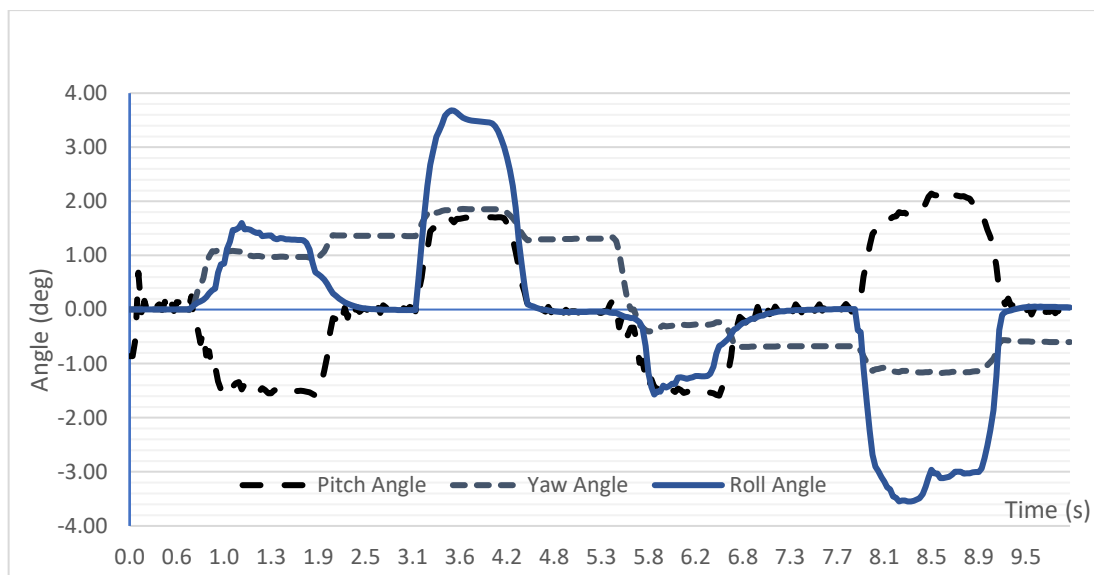


Figure 4.17: Pitch, Yaw, and Roll angle ($^{\circ}$) versus time (s) graph for motion study

First, talking about the pitch angle, the pitch angle when the front wheels pass the barriers is about 1.5 degrees, but when the rear wheels pass the barriers, the pitch angle is about 1.8 degrees. This is mainly due to the stiffness of the spring for the suspension system. Front suspension springs have low stiffness per spring length, making the compression of springs easy to perform, which leads to the smaller pitch angle when passing the barriers.

Next, from Figure 4.17, it is observed that the yaw angle continues to increase on one side from the front wheels passing the left barrier until the rear wheels pass the left barrier. This situation remains the same when it passes the right barrier, just in a different direction. The suspected reason for this problem is that when each wheel climbs up the barrier, some slipping between the wheel and the barrier surface occurs, leading to an increase in yaw angle and the direction of the robot changing as well.

From Figure 4.17 too, the roll angle is observed to have the largest change between the front wheels passing barriers and the rear wheels passing barriers. The roll for the front wheels passing barriers has an angle of about 1.5 degrees on both sides. But it reaches about 3.5 degrees on both sides when the rear wheels pass the barriers. The reason is because of the stiffness of the spring for suspension systems, which is the same as the reason stated in the pitch angle explanation.

4.5.2 Mobility test run

In this real-case mobility test run, two barriers that were designed for the motion study are printed out and used for this test to determine whether the prototype can pass all the barriers and to verify the results obtained from the motion study above. Figure 4.18 shows the video snapshot of the prototype passing barriers. As a result, the prototype was able to pass through all the barriers stably. Besides, it also did not overturn in the middle of the test.



Figure 4.18: The prototype passes two barriers on the left and right sides (side view)

It is difficult for this mobility test run to be verified with the motion study results as the values of those angles cannot be obtained from the test run. The only way to verify the results is to illustrate them using diagrams. The pitch of the prototype can be observed from Figure 4.18. It was observed that for all four barriers passing, the whole prototype was tilting upward and downward accordingly. While for the yaw and roll of the prototype, these results were observed from Figure 4.19. For the prototype roll, roll was observed but with no obvious differences between the front wheels and rear wheels passing the barriers. As for the prototype yaw, the prototype gives an obvious result on it. As from Figure 4.19, the direction of the whole prototype is slightly left after passing the left barriers. After that, the yaw direction changes to right immediately when the right front wheel climbs up the barrier. The yaw direction

further increases to the right when the right rear wheel passes the barrier, and the prototype keeps right after the test run. With this result, it is enough to say that the mobility test run is verified.

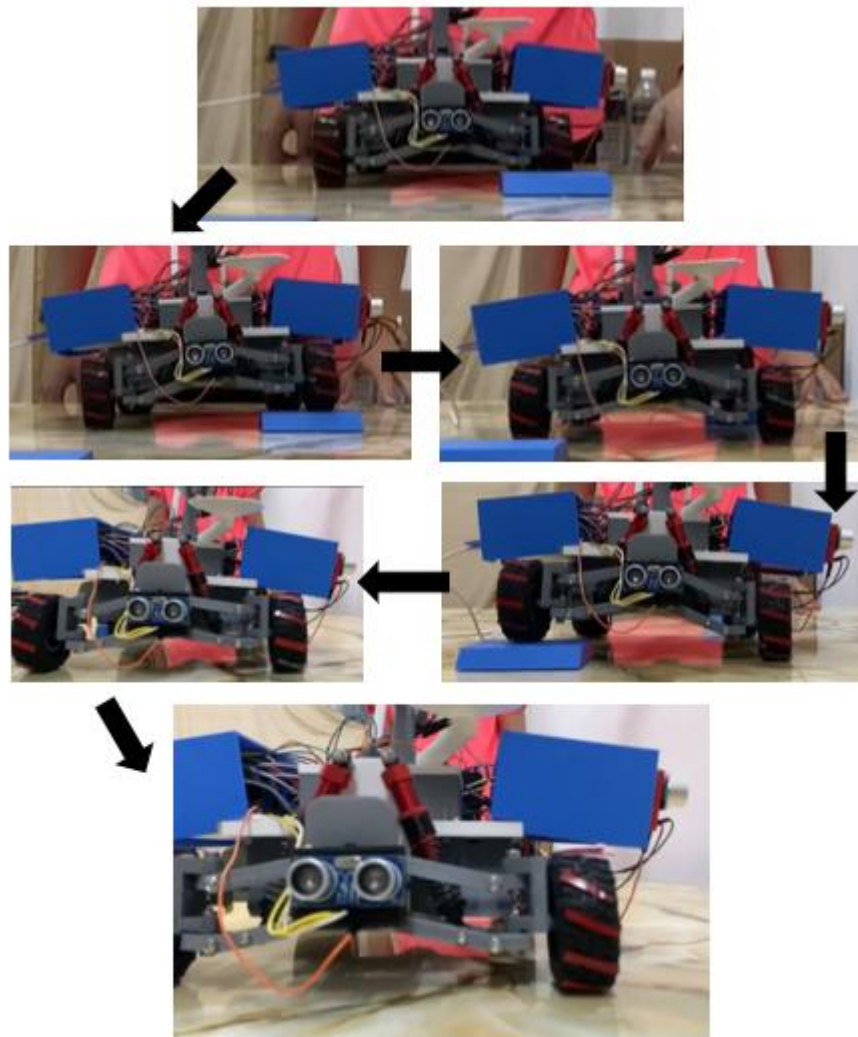


Figure 4.19: The prototype passes two barriers on the left and right sides (front view)

4.6 Key Findings

A latex cup collector robot was designed, and its prototype was fabricated by a 3D printer. The prototype is 285 mm in length, 290 mm in width, and 270 mm in height. Besides, it weighs 2266 grammes. It was made up of a mobility subsystem, a manipulator subsystem, a latex tank, and a platform.

Two parts of the prototype (robot platform and robotic arm) that experience large forces and loads are done with the FEA simulation. The robotic platform experiences maximum stress, displacement, and strain of 2.589×10^6 N/m², 1.494×10^{-1} mm, and 3.551×10^{-1} mm/mm, respectively. A robotic arm has a maximum stress of 8.676×10^5 N/m², a maximum displacement of 1.868×10^{-1} mm, and a maximum strain of 1.683×10^{-1} mm/mm. As a result, both parts won't fail under all expected scenarios because the maximum stress experienced by these two did not exceed the PLA plastics' yield strength of 7.000×10^7 N/m². The results are proven since the prototype can be assembled and perform all the test runs.

Next, the topple angles of the prototype in four different scenarios were calculated using the centre of mass obtained from the Solidworks software. These topple angles were then verified through experiments. But only two scenarios were involved so as to prevent water spillage during the experiment. Percentage errors between calculated and experimental results were calculated, and the amount of percentage errors was discussed. As a result, the prototype can encounter an incline with a minimum angle of 39° when enough power is supplied to the prototype.

In the prototype test run, the prototype worked well in both the functional test and the manipulator test. The prototype takes 106.5 seconds to complete a working cycle from tree sensing, turning into the tree, latex cup collecting, and reserving back to the track. Besides, the robotic arm designed is also able to collect latex cups with different height settings (160 mm, 120 mm, and 105 mm). Lastly, the prototype also performs well in the mobility test. It is able to cross two 15 mm high barriers that are located on both the left and right sides of the prototype with small angles of pitch, yaw, and roll as well as without prototype overturn.

CHAPTER 5

CONCLUSION AND RECOMMENDATIONS

5.1 Conclusion

In conclusion, all the objectives of this project have been achieved. A latex cup robot collector robot was designed, and its prototype was fabricated by the 3D printer. It consists of a rear-wheel-drive transmission system, an Ackerman steering system, double wishbone, and spring suspension systems, as well as a 4 DoF robotic arm manipulator. The designed prototype was able to travel in the simplified, unstructured terrain and also collect the latex cups that were placed at different heights on the rubber tree. Several analyses and tests have been conducted to test the practicality and functionality of the robot prototype. Static tests and toppling analysis were done to determine the mechanical stability of the prototype, while the functional test, the manipulation test, and mobility test were also conducted to test for the suitability of component designs and firmware chosen for the prototype when it carries out the tasks. As the results show, all the tests and experiments showed good results for the prototype, as it did not fail or overturn in the static or dynamic state.

5.2 Recommendations

Throughout the working process on this design and its prototype, several problems came up, and some ideas, suggestions, and recommendations were prompted to improve the current design for future work.

Firstly, the transmission system of the robot should be changed to all-wheel drive instead of differential rear-wheel drive. The steering also needs to be changed from Ackerman steer to skid steer. Although the rear-wheel drive can save the amount of motor usage to drive the robot, Ackerman steering can keep the wheels from spoiling to prevent maintenance costs. However, the combination of these systems requires large spaces to perform the turning, and this eventually takes longer time to perform the task. Thus, all-wheel-drive and skid steer can reduce the cycle time of the work, but at the opportunity cost of increasing the budget.

An alternative way to tackle the problem stated above is to add one DoF (left and right movement) to the robotic arm while the transmission system sticks to its current design. The working concept will be to put the robot perpendicular to the rubber tree. The robot transmission only needs to keep travelling straight while letting the robotic arm perform all the tasks (turn left or right to reach the rubber tree, extend the arm to reach the latex cups, and so on) when reaching the rubber tree. By this, the robot not only reduces the time spent on turning, but the cost of buying extra motors and repairing the worn wheels can be saved.

REFERENCES

- Abdullah, M.S., Abdullah, A.B. and Samad, Z., 2019. Structural integrity assessment of a composite joint: A review. In: A.B. Abdullah and S.M. Sapuan, eds. 2019. *Hole-Making and Drilling Technology for Composites*. Woodhead Publishing. pp. 31-46. Available at: <<https://doi.org/10.1016/B978-0-08-102397-6.00003-9>> [Accessed 23 March 2022]
- Anon, n.d. *Ackerman? Anti-Ackerman? Or Parallel Steering?* [online] . Available at: <https://www.me.ua.edu/me364/PDF/Steering_Ackerman.pdf>. [Accessed 29 Jul. 2021].
- AlSahlani, A., Khashan, M.K. and Khaleel, H.H., 2018. Design and analysis of coil spring in vehicles using finite elements method. *International Journal of Mechanical and Production Engineering Research and Development*, [online] 8(4), pp.615-624. Available at: <https://scholar.google.com/scholar?as_q=DESIGN+AND+ANALYSIS+OF+COIL+SPRING+IN+VEHICLES+USING+FINITE+ELEMENTS+METHOD> [Accessed 13 July 2021]
- Anjum, S., Kamal, N., Khan, U.S., Iqbal, J., Izhar, U., Rasheed, N. and Khan, M.A., 2012, October. *Design of non-conventional chain drive mechanism for a mini robot*. In: 2012 International Conference of Robotics and Artificial Intelligence, pp. 103-107. IEEE. <https://doi.org/10.1109/ICRAI.2012.6413403> [Accessed 13 July 2021]
- AZO Materials, 2006. *Natural Rubber / Latex – Production of Natural Rubber*. [online] Available at: <<https://www.azom.com/article.aspx?ArticleID=3580>>. [Accessed 2 August 2021]
- Bhattacharya, P. and Gavrilova, L.M., 2008. Roadmap-Based Path Planning - Using the Voronoi Diagram for a Clearance-Based Shortest Path. *IEEE Robotics & Automation Magazine*, [e-journal] 15(2), pp.58-66. <https://doi.org/10.1109/MRA.2008.921540> [Accessed 16 August 2021]
- Bechar, A. and Vigneault, C., 2016. Agricultural robots for field operations: Concepts and components. *Biosystems Engineering*, [e-journal] 149, pp.94-111. <https://doi.org/10.1016/j.biosystemseng.2016.06.014> [Accessed 5 August 2021]

- Birrell, S., Hughes, J., Cai, J.Y., Iida, F., 2020 A field-tested robotic harvesting system for iceberg lettuce. *Journal of Field Robot*, [e-journal], 37, pp.225–245. <https://doi.org/10.1002/rob.21888> [Accessed 5 August 2021]
- Bloch, V., Bechar, A. and Degani, A., 2017. Development of an environment characterization methodology for optimal design of an agricultural robot. *Industrial Robot: An International Journal*, [e-journal] 44(1), pp.94–103. <https://doi.org/10.1108/IR-03-2016-0113> [Accessed 23 June 2021]
- Bochtis, D.D., Sørensen, C.G.C. and Busato, P., 2014. Advances in agricultural machinery management: A review. *Biosystems Engineering*, [e-journal] 126, pp.69–81. <https://doi.org/10.1016/j.biosystemseng.2014.07.012> [Accessed 11 Dec. 2021].
- Bruzzone, L. and Quaglia, G., 2012. Review article: locomotion systems for ground mobile robots in unstructured environments. *Mechanical sciences*, [e-journal] 3(2), pp.49-62. <https://doi.org/10.5194/ms-3-49-2012> [Accessed 15 July 2021]
- Business Wire, 2020. *South East Asia Rubber Markets, 2019-2020 Featuring Bridgestone, Michelin, Goodyear, Continental, Sumitomo Rubber Industries, Thai Rubber Latex (Thaitex) and Fenner - ResearchAndMarkets.com*. [online] Available at:
<<https://www.businesswire.com/news/home/20200427005431/en/South-East-Asia-Rubber-Markets-2019-2020-Featuring-Bridgestone-Michelin-Goodyear-Continental-Sumitomo-Rubber-Industries-Thai-Rubber-Latex-Thaitex-and-Fenner---ResearchAndMarkets.com>> [Accessed 17 August 2021].
- Carlo, F. (2018). *EEZYbotARM MK2*. EEZYrobots [online]. Available at:
<http://www.eezyrobots.it/eba_mk2.html#> [Accessed 9 July 2021]
- Cambridge University Press, 1999. *Cambridge Dictionary*. London: Cambridge University Press (UK). Available at:
<<https://dictionary.cambridge.org/dictionary/english/robot>> [Accessed 2 July 2021]
- Canning, J.R., Edwards, D.B. and Anderson, M.J., 2004. Development of a fuzzy logic controller for autonomous forest path navigation. *Transactions of the ASAE*, [e-journal] 47(1), pp.301-310. <https://doi:10.13031/2013.15855> [Accessed 1 September 2021]
- Ceres, R., Pons, J.L., Jiménez, A.R., Martín, J.M., Calderón, L., 1998. Design and implementation of an aided fruit-harvesting robot (Agribot). *Industrial Robot*, [e-journal] 25(5), pp.337–346. <https://doi.org/10.1108/01439919810232440> [Accessed September 2021]
- Department of Agriculture, 2014. *Australian Vegetable Growing Farms: An Economic Survey, 2012-13 and 2013-14*. [pdf] Australia: Department of Agriculture. Available at:
<http://data.daff.gov.au/data/warehouse/9aab/9aabf/2014/avfesd9absf20141114/AustVegGrwFrmEcoSurvey20141114_1.0.0.pdf> [Accessed 10 July 2021].

- DeSantis, R.M., 1995. Modeling and path-tracking control of a mobile wheeled robot with a differential drive. *Robotica*, [e-journal] 13(4), pp.401–410. <https://doi.org/10.1017/S026357470001883X> [Accessed 20 August 2021]
- Doi, M.A.C., Yusuff, R.M. and Leman, Z., 2014. A preliminary study of prevalence of musculoskeletal disorders among Malaysian Rubber Tappers. *Age*, 45, [online] pp.25-78. Available at: <https://scholar.google.com/scholar?hl=en&as_sdt=0%2C5&q=A+preliminary+study+of+prevalence+of+musculoskeletal+disorders+among+Malaysian+Rubber+Tappers&btnG=>> [Accessed July 12 2021].
- de Livonnière, H., 1993. Industrial natural rubber collection and control procedures. *Clinical reviews in allergy*, [e-journal] 11(3), pp.309-323. <https://doi.org/10.1007/BF02914414> [Accessed 19 August 2021]
- Encyclopaedia Britannica., n.d. *Rubber*. [online] Available at: <https://www.britannica.com/science/rubber-chemical-compound/additional-info#full_index> [Accessed 17 July 2021].
- Energy Education, n.d. *Drive shaft*. [online] Available at: <https://energyeducation.ca/encyclopedia/Drive_shaft> [Accessed 29 Jul. 2021].
- Food and Agriculture Organization (FAO), 1977. *Tapping*. [online] Available at: <<https://www.fao.org/3/AD221E/AD221E06.htm#ch6>> [Accessed 14 July 2021]
- Fauroux, J.C. and Bouzgarrou, B.C., 2011. Dynamic obstacle-crossing of a wheeled rover with double-wishbone suspension. *Field Robotics*, [e-journal] pp. 642-649. https://doi.org/10.1142/9789814374286_0075 [Accessed 27 July 2021]
- Fue, K.G., Porter, W.M., Barnes, E.M. and Rains, G.C., 2020. An extensive review of mobile agricultural robotics for field operations: focus on cotton harvesting. *AgriEngineering*, 2(1), [e-journal] pp.150-174. <https://doi.org/10.3390/agriengineering2010010> [Accessed 25 August 2021]
- Ge, Y., Xiong, Y., Tenorio, G.L., From, P.J., 2019. Fruit Localization and Environment Perception for Strawberry Harvesting Robots. *IEEE Access*, [e-journal] 7, pp. 147642–147652. <https://doi.org/10.1109/ACCESS.2019.2946369> [Accessed 25 August 2021]
- Giang, K., n.d. *PLA vs ABS: What's the difference?* [Online]. Available at: <<https://www.3dhubs.com/knowledge-base/pla-vs-abs-whats-difference/>> [Accessed 27 October 2021]
- Gonzalez, C., 2015. *An overview on the differences between powered actuators and their benefits*. *MachineDesign* [online] Available at: <<https://www.machinedesign.com/mechanical-motion-systems/linear-motion/article/21832047/whats-the-difference-between-pneumatic-hydraulic-and-electrical-actuators.>> [Accessed 29 July 2021]

- Hayashi, S., Yamamoto, S., Saito, S., Ochiai, Y., Kamata, J., Kurita, M., Yamamoto, K., 2014. Field Operation of a Movable Strawberry harvesting Robot using a Travel Platform. *Japan Agricultural Research Quarterly*, [e-journal] 48, pp.307–316. <https://doi.org/10.6090/jarq.48.307> [Accessed 29 July 2021]
- Hegde, R., Yogesh, G. and Chawhan, S., 2018. Comparative Study on Rectangular and Circular Water Tank using STAAD Pro Software. *International Research Journal of Engineering and Technology*, [online] Available at: <<https://www.irjet.net/archives/V5/i11/IRJET-V5I11255.pdf>> [Accessed 29 July 2021].
- Hoogewijs, D., 2020. *Research and design of an autonomous and collaborative guided vehicle prototype, to be applied in indoor and outdoor environments and different types of floor*. [online]. Available at: <<https://repositorio.ufscar.br/handle/ufscar/13994>> [Accessed 20 July 2021]
- Hrbáček, J., Ripel, T. and Krejsa, J., 2010. *Ackermann mobile robot chassis with independent rear wheel drives*. Proceedings of 14th International Power Electronics and Motion Control Conference EPE-PEMC 2010, Ohrid, Macedonia, 6-8 September 2010. <https://doi.org/10.1109/EPEPEMC.2010.5606853> [Accessed 25 July 2021]
- Kim, I., Jeon, W. and Yang, H., 2017. Design of a transformable mobile robot for enhancing mobility. *International Journal of Advanced Robotic Systems*, [e-journal] 14(1). <https://doi.org/10.1177%2F1729881416687135> [Accessed 25 July 2021]
- Kitagawa, H., Ohno, T., Miyoshi, T. and Terashima, K., 2009. Development of Differential-Drive Steering System for Omnidirectional Mobile Robot. *Journal of the Robotics Society of Japan*, 27(3), pp.343–349.
- Kondo, N. and Ting, K.C., 1998. *Robotics for Plant Production*. Artificial Intelligence Review, [e-journal] 12, pp.227–243. Available at: <<https://doi.org/10.1023/A:1006585732197>> [Accessed 15 July 2021]
- Kozłowski, K. and Pazderski, D., 2004. *Modeling and control of a 4-wheel skid-steering mobile robot*. International journal of applied mathematics and computer science, [e-journal] 14(4), pp.477-496. Available at: <<http://zbc.uz.zgora.pl/Content/2576/HTML/5kozl.pdf>> [Accessed 15 July 2021]
- Liné, 2020. *Latex vs Rubber. Is it the same thing?* [online] Available at: <<https://ecoworldonline.com/latex-vs-rubber-is-it-the-same-thing/>> [Accessed 2 August 2021]
- LittleCraft, n.d. *Arduino N20 Mini DC Motor with Gear Head - 30, 60, 100RPM DC12V \ Shopee Malaysia*. [online] Available at: <<https://shopee.com.my/Arduino-N20-Mini-DC-Motor-With-Gear-Head-30-60-100RPM-DC12V-i.6674515.423382054>> [Accessed 10 November 2021]
- Logsdon, T., 2000. *The Robot Revolution*. iUniverse. Available at: <<https://books.google.com.my/books?id=FB-yg7s9bF0C&printsec=>

frontcover&dq=The+Robot+Revolution&hl=en&sa=X&redir_esc=y#v=onepage
&q=The%20Robot%20Revolution&f=false> [Accessed 2 July 2021]

- Lowenberg-DeBoer, J.M., and Erickson, B., 2019. *Setting the Record Straight on Precision Agriculture Adoption*. *Agronomy Journal*, [e-journal] 111, pp. 1552–1569. <https://doi.org/10.2134/agronj2018.12.0779> [Accessed 5 July 2021]
- Lundström, G., 1974. *Industrial Robot Gripper*. *Industrial Robot: An International Journal*, [e-journal] 1(2), pp.72 – 82. <https://doi.org/10.1108/eb004449> [Accessed 5 July 2021]
- Manikandan, K. and Srinivasan, S., 2014. Composition of Agricultural Robotic Technology. *International Journal of Agriculture & Environmental Science*, 1(1), pp.11–15.
- Marinoudi, V., Sørensen, C.G., Pearson, S. and Bochtis, D., 2019. Robotics and labour in agriculture. A context consideration. *Biosystems Engineering*, [online] Available at:
<<https://www.sciencedirect.com/science/article/pii/S1537511019303617>>
[Accessed 13 Mar. 2020].
- Matweb., 2020. Overview of materials for Polylactic Acid (PLA) Biopolymer [Online]. Available at:
<<http://www.matweb.com/search/DataSheet.aspx?MatGUID=ab96a4c0655c4018a8785ac4031b9278>> (Accessed: August 2020)
- Megalingam, R.K., Kuttankulangara Manoharan, S., Mohan, S.M., Vadivel, S.R.R., Gangireddy, R., Ghanta, S., Kotte, S., Perugupally, S.T., Sivanantham, V. Amaran., 2020. An Unmanned Robotic Coconut Tree Climber and Harvester. *IEEE/ASME Trans. Mechatron*, [e-journal] 26, pp.288–299.
- Malayan Rubber Council (MRC), 2021. *Industry Overview*. [online]. Available at:
<http://www.myrubbercouncil.com/industry/malaysia_production.php> [Accessed 17 Aug. 2021].
- Monta, M., Kondo, N. and Ting, K.C., 1998. End-effectors for tomato harvesting robot. *Artificial Intelligence for Biology and Agriculture*, [e-journal] pp. 1-25. https://doi.org/10.1007/978-94-011-5048-4_1 [Accessed 22 September 2021]
- Nakajima, S., 2011. *RT-Mover: a rough terrain mobile robot with a simple leg–wheel hybrid mechanism*. *The International Journal of Robotics Research*, [e-journal] 30(13), pp.1609–1626. <https://doi.org/10.1177%2F0278364911405697> [Accessed 28 September 2021]
- Neal, A.J., n.d. Tips for Selecting DC Motors For Your Mobile Robot. *Servo Magazine* blog, [blog] Available at:
<https://www.servomagazine.com/magazine/article/tips_for_selecting_dc_motors_for_your_mobile_robot#> [Accessed 24 July 2021]

- Ng, K.C. and Trivedi, M.M., 1998. A neuro-fuzzy controller for mobile robot navigation and multirobot convoying. *IEEE Transactions on Systems, Man, and Cybernetics, Part B (Cybernetics)*, [e-journal] 28(6), pp.829-840. <https://doi.org/10.1109/3477.735392> [Accessed 30 October 2021]
- Oliveira, L.F., Moreira, A.P. and Silva, M.F., 2021. Advances in agriculture robotics: A state-of-the-art review and challenges ahead. *Robotics*, [e-journal] 10(2), pp.52. <https://doi.org/10.3390/robotics10020052> [Accessed 15 July 2021]
- Pant, R., Joshi, J., Kumar, P. and Patil, P.P., 2019. Agricultural Robot: The Needs and Limitations of Large-Scale Commercialization. *Journal of Critical Reviews*, [online]. Available at: < https://www.researchgate.net/profile/Jyoti-Joshi-16/publication/351578094_AGRICULTURAL_ROBOTS_THE_NEEDS_AND_LIMITATIONS_IN_LARGE_SCALE_COMMERCIALIZATION/links/609e3b26458515c2658d5961/AGRICULTURAL-ROBOTS-THE-NEEDS-AND-LIMITATIONS-IN-LARGE-SCALE-COMMERCIALIZATION.pdf > [Accessed 15 August 2021]
- Pastor, R., Vysocky, A., Siroky, P., Konecny, Z. and Karnik, L., 2018. Use of different simulation methods for design of experimental rover. *MM Science Journal*, [e-journal] 12(2018), pp.2616–2620. [Accessed 17 August 2021]
- Qi, D., Zhou, J., Xie, G. & Wu, Z. 2015. ‘Optimizing Tapping-Tree Density of Rubber (*Hevea brasiliensis*) Plantations in South China’. *Small Scale Forestry*, 15(1), pp. 61–72. <https://doi.org/10.1007/s11842-015-9308-8> [Accessed 26 Jul. 2021].
- Quora.com., n.d. Alek Eccles’s answer to Why is a water tank square and not cylindrical? - Quora. [online] Available at: <<https://www.quora.com/Why-is-a-water-tank-square-and-not-cylindrical/answer/Alek-Eccles>> [Accessed 29 Jul. 2021].
- Quora.com., n.d. Jim Urdu’s answer to Why is a water tank square and not cylindrical? - Quora. [online] Available at: <<https://www.quora.com/Why-is-a-water-tank-square-and-not-cylindrical/answer/Jim-Urdu>> [Accessed 29 Jul. 2021].
- Roh, S.G., Lim, B., Moon, H., Lee, J.S., Park, J.H., Koo, J.C. and Choi, H.R., 2013. *Flexible suspension mechanism for stable driving of a differential drive mobile robot*. In 2013 IEEE/RSJ International Conference on Intelligent Robots and Systems, pp.5518-5523. [Accessed 17 August 2021]
- Sacrewell Farm., 2017. *Why do tractors have smaller wheels at the front and larger wheels at the back?* [online] Available at: <<https://www.sacrewell.org.uk/news/why-do-tractors-have-smaller-wheels-at-the-front-and-larger-wheels-at-the-back/>> [Accessed 14 Aug. 2021].
- Saraiya, P.B., 2020. Design of Rocker Bogie Mechanism. *International Research Journal of Engineering and Technology (IRJET)*, [online] 07(08). Available at: <<https://www.irjet.net/archives/V7/i8/IRJET-V7I8255.pdf>> [Accessed 29 Jul. 2021].

- Silva, M.F. and Machado, J.T., 2011. A literature review on the optimization of legged robots. *Journal of Vibration and Control*, [e-journal] 18(12), pp.1753–1767. <https://doi.org/10.1177%2F1077546311403180> [Accessed 22 July 2021]
- SGrobot, n.d. *A58SW-555 12V Worm Gear High Speed & Torque DC Motor \ Shopee Malaysia* [online] Available at: < <https://shopee.com.my/A58SW-555-12V-Worm-Gear-High-Speed-Torque-DC-Motor-i.33287405.790990474> > [Accessed 19 November 2021]
- Sundar, S., Sudarsanan, T. and Krishnan, R., 2018. Review of Design and Fabrication of four-wheel Steering system. *International Journal of Recent Trends in Engineering & Research (IJRTER)*, 4(10), pp.1034-1049. [Accessed 24 August 2021]
- Synacorp, n.d. *MG996R MG995 MG996 Metal Gear Servo Motor (High Speed & Torque) & Bracket \ Shopee Malaysia* [online] Available at: < [https://shopee.com.my/MG996R-MG995-MG996-Metal-Gear-Servo-Motor-\(High-Speed-Torque\)-Bracket-i.23949362.1377760744](https://shopee.com.my/MG996R-MG995-MG996-Metal-Gear-Servo-Motor-(High-Speed-Torque)-Bracket-i.23949362.1377760744) > [Accessed 12 November 2021]
- Synacorp, n.d. *SG90 MG90 TS90A Tower Pro Micro Servo Motor 180d MG90s SG90s TS90 \ Shopee Malaysia* [online] Available at: < <https://shopee.com.my/SG90-MG90-S-Tower-Pro-Micro-Servo-Motor-180d-i.23949362.858777215> > [Accessed 12 November 2021]
- Tan, V., 2020. *Malaysia's glove industry is booming amid COVID-19, but are rubber smallholders seeing the benefits?* CNA, [online] 9 October. Available at: < <https://www.channelnewsasia.com/asia/malaysia-rubber-industry-gloves-trickle-down-smallholder-covid19-601401> > [Accessed 10 July 2021]
- The Edge Markets., 2020. *Cover Story: Diverging paths in Malaysia's rubber industry.* [online] Available at: < <https://www.theedgemarkets.com/article/cover-story-diverging-paths-malaysias-rubber-industry> > [Accessed 15 July 2021].
- Townsend, B., 2002. *Static and kinetic friction.* [online] Available at: < http://ffden-2.phys.uaf.edu/211_fall2002.web.dir/ben_townsend/StaticandKineticFriction.htm > [Accessed 24 November 2021]
- Ueno, Y., Ohno, T., Terashima, K., Kitagawa, H., Funato, K. and Kakihara, K., 2010. *Novel differential drive steering system with energy saving and normal tire using spur gear for an omni-directional mobile robot.* 2010 IEEE International Conference on Robotics and Automation. Anchorage, AK, USA.[Accessed 23 August 2021]
- Universal Robots., 2020. *Types of Grippers Used in Manufacturing.* [online] Available at: < <https://www.universal-robots.com/blog/types-of-grippers-used-in-manufacturing/> > [Accessed 30 July 2021]
- Wacme Pty Ltd., 2021. *What Makes Cylindrical-Shaped Water Tanks Suitable for Liquid Transport.* [online] Available at: < <https://wet1.com.au/what-makes->

cylindrical-shaped-water-tanks-suitable-for-liquid-transport/.> [Accessed 2 August 2021]

- Wang, T., Wu, Y., Liang, J., Han, C., Chen, J. and Zhao, Q., 2015. Analysis and Experimental Kinematics of a Skid-Steering Wheeled Robot Based on a Laser Scanner Sensor. *Sensors*, [e-journal] 15(5), pp.9681–9702. <https://doi.org/10.3390/s150509681> [13 August 2021]
- Wickramanayake, P.N., 2020. *Hybrid locomotion for agricultural robotic platform*. [online] Available at: <<https://mro.massey.ac.nz/bitstream/handle/10179/15952/WickramanayakeMETHesis.pdf?sequence=1&isAllowed=y>> [Accessed 23 Aug. 2021].
- Yadav, N., Bhardwaj, B. and Bhardwaj, S., 2015. Design analysis of Rocker Bogie Suspension System and Access the possibility to implement in Front Loading Vehicles. *IOSR Journal of Mechanical and Civil Engineering*, 12(3), pp.64-67. [Accessed 3 September 2021]
- Yaghoubi, S., Akbarzadeh, N. A., Bazargani, S. S., Bazargani, S. S., Bamizan, M., Asl, M. I., 2013. Autonomous robots for agricultural tasks and farm assignment and future trends in agro robots. *International Journal of Mechanical and Mechatronics Engineering*, [online] Available at: <<https://elibrary.asabe.org/abstract.asp?aid=15855>> [Accessed 12 July 2021]
- Zhao, Y., Gong, L., Huang, Y., & Liu, C., 2016. *Robust tomato recognition for robotic harvesting using feature images fusion*. *Sensors*, 16(2), pp.173. <https://doi.org/10.3390/s16020173> [Accessed 7 August 2021]
- Zhang, F., Wang, Y., Teng, S., Zheng, L., Wang, J. and Chen, Z., 2019. Development of agricultural bionic four-legged robot: Effect of head movement adjustment on the stability of goats. *International Journal of Agricultural and Biological Engineering*, [online] Available at: <<http://www.ijabe.org/index.php/ijabe/article/view/4287>> [Accessed 18 July 2021]